Marine Structures 51 (2017) 87–109

Contents lists available at ScienceDirect

Marine Structures

journal homepage: www.elsevier.com/locate/marstruc

Development and verification of a time-domain approach for determining forces and moments in structural components of floaters with an application to floating wind turbines

Chenyu Luan [a, *], Zhen Gao [b], Torgeir Moan [c]

[a] Norwegian Research Centre for Offshore Wind Technology (NOWITECH), Centre for Ships and Ocean Structures (CeSOS), NTNU, Centre for Autonomous Marine Operations and Systems (AMOS), NTNU, NO-7491 Trondheim, Norway
[b] CeSOS and AMOS, NTNU, Department of Marine Technology, NTNU, NO-7491 Trondheim, Norway
[c] CeSOS and AMOS, NTNU, NOWITECH, Department of Marine Technology, NTNU, NO-7491 Trondheim, Norway

ARTICLE INFO

Article history:
Received 25 May 2016
Received in revised form 23 August 2016
Accepted 7 October 2016
Available online 24 October 2016

ABSTRACT

Structural design of the floater is an important aspect in developing cost efficient and reliable floating wind turbines. It is difficult to well account for the effect of strong non-linear dynamic characteristics and transient loading events, e.g. wind turbine faults, of floating wind turbines in a frequency-domain finite element analysis. The time-domain approach which implements the Morison's formula cannot accurately account for the hydrodynamic loads on the hull of floating wind turbines. While, the conventional hybrid frequency-time domain approach (based on the potential flow theory) fails to capture structural responses of the hulls since a rigid-body global model rather than a finite element model of the hull is employed. The present paper deals with the development and verification of a time-domain approach that can be easily implemented in various state-of-the-art computer codes for wind turbine analysis, e.g. Simo/Riflex/Aerodyn, OrcaFlex and FAST + CHARM3D, to extend their capabilities to analyze global forces and moments in structural components of a generic floater subject environmental loads from e.g. wind and waves. The global forces and moments in the structural components might be used as inputs of design formulas for structural strength design checks and/or used as boundary conditions in a sub-model finite element analysis to determine structural responses such as stresses. The proposed approach focuses on modeling of the inertia and external loads on the hull and mapping of the loads in the finite element model of the hull. In the proposed approach, floating wind turbines are considered as a system of several structural components, e.g. blades, rotational shaft, nacelle, tower, mooring lines, columns, pontoons and braces, rather than one rigid-body, while a finite element model for the hull is developed to represent the global stiffness of the structural components. The external and inertial loads on the hull are modeled as distributed loads rather than the integrated forces and moments. The conventional hybrid frequency-time domain approach, which is available in the state-of-the-art computer codes, is implemented to model the hydrodynamic loads on each structural component with essential modifications with respect to the corresponding hydrodynamic coefficients, e.g. added mass and potential damping coefficients and wave excitation forces. Approaches for modeling the hydrostatic pressure forces, gravity loads, drag forces and inertial loads on each structural component are also illustrated. Second order and higher order terms of the hydrostatic and hydrodynamic loads and the hydroelasticity effects are not accounted for in the present paper but can be

* Corresponding author.
E-mail addresses: chenyu.luan@ntnu.no (C. Luan), zhen.gao@ntnu.no (Z. Gao), torgeir.moan@ntnu.no (T. Moan).

http://dx.doi.org/10.1016/j.marstruc.2016.10.002

further included. So far, the proposed approach has been implemented in the computer code Simo/Riflex/Aerodyn to analyze global forces and moments in the hull of a semi-submersible wind turbine. Good agreement between the reference values and the simulation results has been observed and indicates that the developed time-domain numerical models are reliable. The simulation results show that the low-frequency aerodynamic loads and fluctuations of hydrostatic pressure forces on and gravity of the floating wind turbine are important contributions to the structural responses, in particular, in the low-frequency range.

1. Introduction

By now, onshore wind energy has been well developed while the potential of offshore wind energy is substantial, particularly in relatively deep water (e.g. deeper than 80 m). Moving from onshore and shallow water to deep water, floating wind turbines might be more economically competitive than bottom fixed wind turbines in particular for large wind turbines with high rated power (e.g. 5–10 MW).

In general, a floating wind turbine is composed of a Rotor Nacelle Assembly (RNA), a tower, a hull and a mooring system. Current floating wind turbines can be classified as spar-type [1,2], TLP [3–9] and semi-submersible wind turbines [10–17].

In the structural design, ultimate limit state (ULS) and fatigue limit state (FLS) design checks must be carried out based on structural responses of the floating wind turbine in relevant design conditions. Finite element analysis is normally carried out to determine the load effects for the design checks with appropriate models of the loads.

Shell elements might be employed to model structural details, e.g. bulkheads, girders and stiffeners in the hull, blades and tower; chains and wires of the mooring lines; and gear box, shaft and generator in nacelle. Alternatively, we might consider that the structure is composed of several structural components (based on a multi-body formulation). For instance, the blades, rotational shaft, nacelle, tower, mooring lines and columns, pontoons and braces of the hull can be considered as structural components. Beam elements can be used to account for the global structural behaviors of these structural components, e.g. the global forces and moments in the structural components. The global forces and moments might be used as inputs of design formulas for structural strength design checks specified by relevant standards and guidelines from the International Electrotechnical Commission (IEC), International Organization for Standardization (ISO), American Petroleum Institute (API), the Norwegian petroleum industry, class societies such as Det Norske Veritas and Germanischer Lloyd (DNVGL) and the American Bureau of shipping (ABS) and so on. For example, buckling strength of plates, stiffeners and girders in global and local loads can be checked by the formulas specified in DNV-RP-C201 [19]. The global forces and moments might be used in ULS design checks for tubular members and joints based on formulas specified in NORSOK-N004 [20]. In addition, the global forces and moments might be used as boundary conditions in a sub-model finite element analysis to determine structural responses such as stresses, etc.

Finite element analysis in frequency domain is very cost-effective. However, the major limitations are that 1) it is a big challenge to appropriately account for the strong non-linear dynamic characteristics, which is known as the aero-hydro-servo-elastic feature [35], of floating wind turbines; and 2) transient loading events, such as wind turbine faults, cannot be modeled in frequency domain.

Regarding the finite element analysis in time domain, 19 computer codes used by participants from various organizations in several countries were compared through a code-to-code verification activity [22]. However, none of the developed numerical models can be used to predict the global forces and moments in the hull of the reference semi-submersible wind turbine. The challenges are 1) how to accurately calculate hydro loads on the hull and 2) how to effectively map the loads in the finite element model.

As pointed by Matha et al. [36], the Morison's formula, potential flow theory and computational fluid dynamics methods can be used to model hydrodynamic loads on the hull and mooring lines. ULS and FLS design checks require tens of thousands of time-domain simulation hours [37–39]. Therefore, the computational fluid dynamic method is not considered to be practical for ULS and FLS design checks due to the extremely expensive computational cost.

The Morison's formula is implemented in some cost effective computer codes [22] to model the hydrodynamic loads on the hull of floating wind turbines. However, the Morison formula is an empirical formula. In general, it is applicable when wave length is larger than five times the diameter of the slender structure's cross-section [23]. Meanwhile, the application of the Morison formula means the memory effects of the hydrodynamic loads are neglected. In addition, additional pressure forces must be added to account for hydrodynamic loads in axial directions of the columns and pontoons [22].

The potential flow theory combined with the drag term of the Morison formula can accurately model the hydrodynamic loads on offshore structures and is frequently used in the offshore oil and gas industry. A set of equations of motions can be established, as initially proposed by Cummins [25], and solved to obtain the motion responses of the platforms in waves. In these equations, the platform is assumed as one rigid-body with 6 d.o.f.s, while a hybrid frequency-time domain approach is

implemented to convert the frequency dependent hydrodynamic pressure loads due to wave diffraction and radiation to the integrated forces and moments corresponding to these 6 d.o.f.s. While, wind loads on blades and tower are typically considered as distributed loads. This approach has been implemented in some computer codes [22] to analyze structural responses of the RNA, tower and mooring lines and rigid-body motions of the hull of floating wind turbines [21,40–45].

The flow chart of a time-domain numerical model of a generic horizontal axis floating wind turbine which implements the hybrid frequency-time domain approach and is developed in the computer code Simo/Riflex/Aerodyn [29–32] is given in Fig. 1 as an example. The hull of the floating wind turbine is considered as a rigid-body with 6 d.o.f.s, while the tower base and fairleads of the mooring lines rigidly follow the motions of the hull. Six motion equations that are composed of the resultant external loads, e.g. viscous loads, gravity loads and hydro loads, on and inertial loads of the hull are generated in Simo [27] with necessary input, e.g. mass properties of the hull, drag coefficients, hydrodynamic coefficients, i.e. the added-mass coefficient matrices ($\boldsymbol{A}(\omega)$), potential damping coefficient matrices ($\boldsymbol{B}(\omega)$) and first order wave excitation load transfer function ($\boldsymbol{H}_{fw}(\omega)$), and specified forces, moments and restoring stiffness matrix. A finite element model, for which the mooring lines, tower and RNA are modeled as bar and beam elements and coupled to the motion equations of the hull are generated and solved in Riflex [28] with necessary input, e.g. relevant mass and structural properties and drag and added mass coefficients. Aerodyn [32] and a Java controller [31] are coupled to Riflex through a dll file [31] to account for the aerodynamic loads on the RNA and tower, effect of pitch control on aerodynamic loads on the three blades and effect of the generator inside the nacelle on the power production and generator torque. More details are available in the later part of this paper and [47].

The conventional hybrid frequency-time domain approach is considered as the state-of-the-art approach and has been used by researchers, e.g. Refs. [21,43,46,47], to analyze responses of floating wind turbines. However, to calculate structural responses of the hull, we must develop a finite element model of the hull rather than a rigid-body formulation; while, to map the loads in the finite element model, we must develop accurate and effective time-domain approach to model the loads on the hull as distributed loads rather than three integrated forces and moments.

This paper addresses a time-domain approach to deal with the challenges mentioned above. The focus is on the modeling of the inertia and external loads on the floating wind turbine hull and the mapping of the loads to the finite element model of the hull. The proposed approach can be easily implemented in various state-of-the-art computer codes, e.g. Simo/Riflex/Aerodyn, OrcaFlex [22] and FAST + CHARM3D [22], to extend their capabilities to analyze global forces and moments in structural components of a generic floater subject to linear and non-linear environmental loads, e.g. wind and waves. Details of the proposed approach and verification are available in the later part of this paper. An application of the proposed approach for ULS design check for the structural design of the hull of a semi-submersible wind turbine is available in Ref. [15].

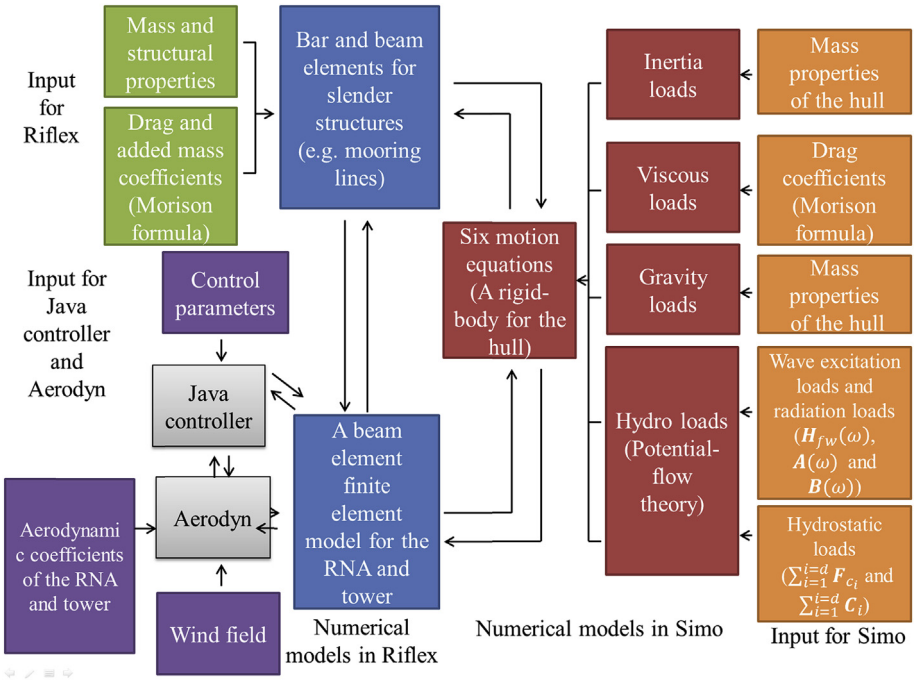

Fig. 1. The flow chart of a time-domain numerical model of a generic horizontal axis floating wind turbine developed in Simo/Riflex/Aerodyn (the conventional approach).

2. The proposed approach

In general, numerical models in finite element codes are developed in an earth fixed coordinate system, such as the global coordinate system (O^g-x^g-y^g-z^g) shown in Fig. 2.

In the proposed approach, the hull of floating structures is considered as an assemble of d structural components. d is specified by designer. A beam element finite element model, which includes d nodes (red colored in Fig. 2), can be developed in the global coordinate system to represent the global stiffness of the structural components. Each node has 6 d.o.f.s and corresponds to a structural component. The external loads on and inertia loads of each structural component are calculated, integrated and transferred to the node that corresponds to the structural component in the finite element model. In particular, the hydrostatic and the hydrodynamic loads on each structural component are obtained by integrating the hydrostatic and hydrodynamic pressure loads on the wet surface of the structural component. The pressure loads are normally calculated based on a frequency-domain hydrodynamic code using a panel method. Global forces and moments in structural components of the hull can be obtained by carrying out a finite element analysis using a time-domain code. Accurate global forces and moments are given at the cross-sections corresponding to the red dashed lines, see Fig. 2. The number of the structural components and quality of the finite element model of the hull affect the accuracy of the global forces and moments. The beam element finite element model of the hull should accurately represent the global stiffness of the hull, in particular for statically indeterminate structures.

The flow chart of a time-domain numerical model of a generic horizontal axis floating wind turbine which implements the proposed approach and is developed in the computer code Simo/Riflex/Aerodyn is given in Fig. 3. Comparing to Fig. 1 (the hybrid frequency-time domain approach), the proposed approach models the hull as a beam element finite element model while the approaches for modeling the external on and inertia loads of each structural component are illustrated in the following part of this section together with the limitations of the approaches.

The approaches are developed by extending the conventional approaches used in the state-of-the-art computer codes. Therefore, the proposed approach can be easily implemented in various state-of-the-art computer codes to extend their capabilities.

Generating and solving time-domain motion equations for a rigid-body oscillating with respect to its mean position in waves is a fundamental feature in some of the state-of-the-art computer codes used in the offshore wind and offshore oil and gas industry. In these computer codes, usually, three coordinate systems, i.e. O^b-x^b-y^b-z^b, O^r-x^r-y^r-z^r and O^f-x^f-y^f-z^f coordinate systems, are established. As shown in Fig. 4, the O^f-x^f-y^f-z^f coordinate system is an earth fixed coordinate system located at the mean position of the geometrical center of the water plane area of the floater. The O^b-x^b-y^b-z^b coordinate system is a body-fixed coordinate system. The position of O^b and the orientation of the coordinate system rigidly follow rigid-body motions of the floater. The O^r-x^r-y^r-z^r coordinate system is a body-related coordinate system. O^r rigidly follows horizontal movements of O^b (the hull) but the orientation of the body-related coordinate system and vertical position of the O^r are fixed (as the same as

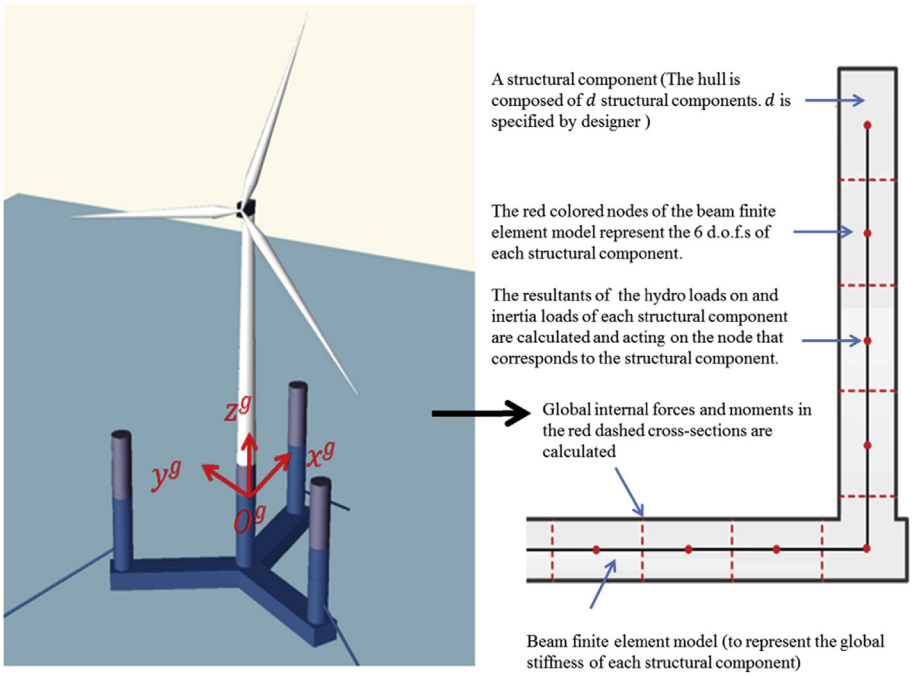

Fig. 2. Definition of a finite element model of the hull.

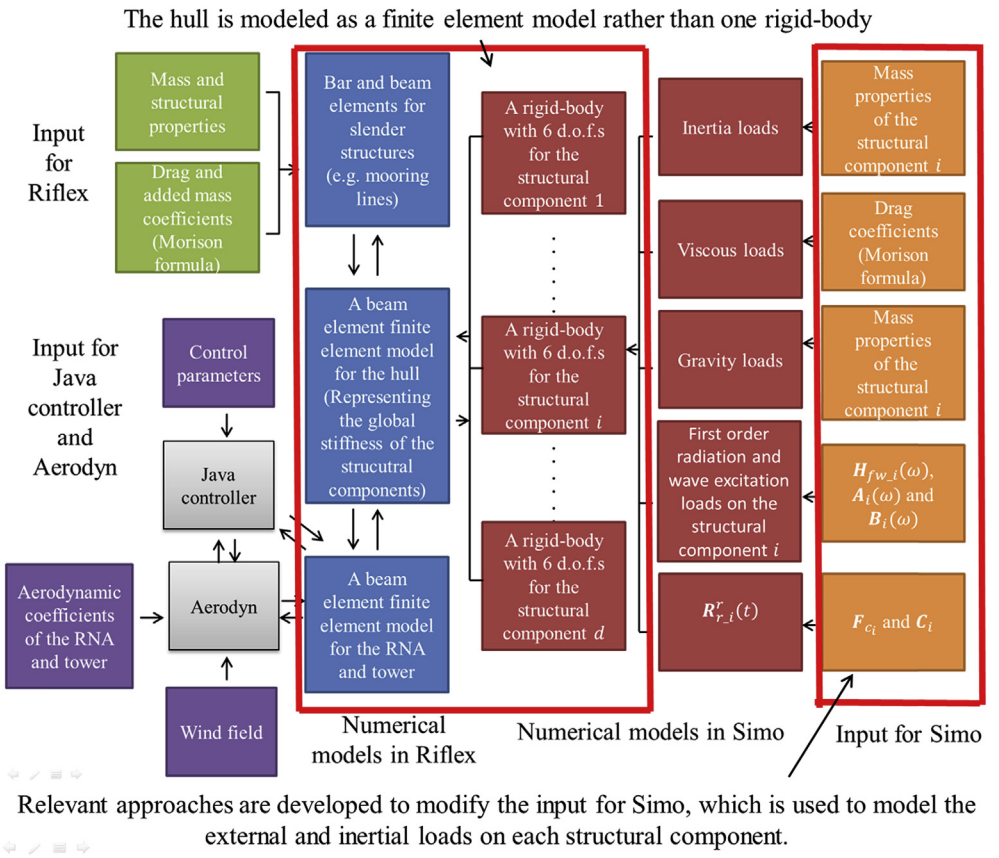

Fig. 3. The flow chart of a time-domain numerical model of a generic horizontal axis floating wind turbine developed in Simo/Riflex/Aerodyn (the proposed approach).

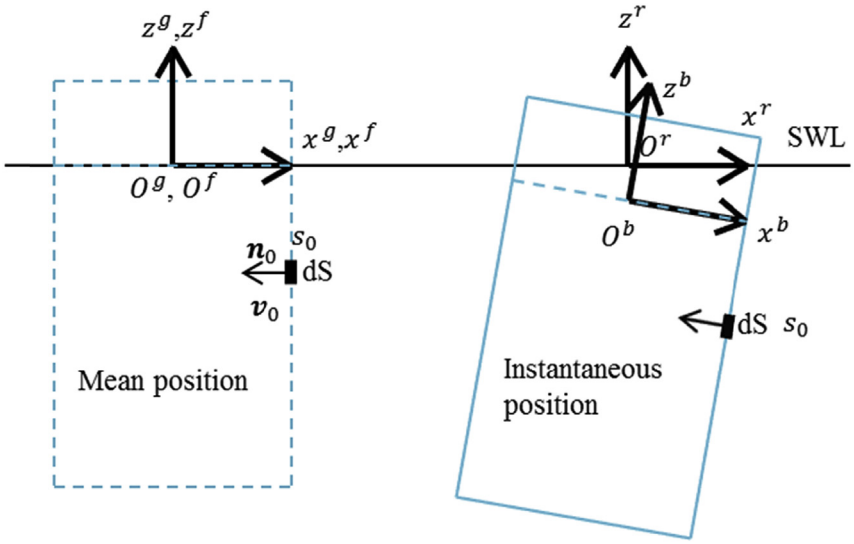

Fig. 4. Definition of the coordinate systems for a floating body.

the body-related coordinate system when the hull is located at its initial position in time-domain simulation). When the floater is located at its mean position, the O^f-x^f-y^f-z^f, O^b-x^b-y^b-z^b and O^r-x^r-y^r-z^r coordinate systems are coincident. In the motion equations, the hybrid frequency-time domain approach is implemented to account for the wave excitation load effects

and radiation load effects on the rigid-body motions. Hydrodynamic coefficients, i.e. the added-mass coefficient matrices ($\boldsymbol{A}(\omega)$), potential damping coefficient matrices ($\boldsymbol{B}(\omega)$) and first order wave excitation load transfer function ($\boldsymbol{H}_{fw}(\omega)$) must be calculated by 1) solving the potential-flow boundary value problem with the assumption that the hull of the floater is a rigid-body in the O^f-x^f-y^f-z^f coordinate system, 2) calculating pressure forces on the mean wet surface of the hull based on the Bernoulli's equation and corresponding velocity potential, 3) integrating the pressure on the wet surface of the hull using the coordinate system O^f-x^f-y^f-z^f to obtain the integrated forces and moments acting on O^f, and 4) derive the hydrodynamic coefficients based on the corresponding resultant forces and moments on the O^f in the O^f-x^f-y^f-z^f coordinate system.

In the proposed approach to calculate external and inertial loads on each structural component, we assumes that 1) the atmospheric pressure inside the hull is constantly equal to the atmosphere pressure at the still water plane and 2) the ballast fluid inside the hull is considered as ballast mass which introduce inertia loads on the hull rather than hydro pressure forces on the corresponding inner surface of the hull; while, in the boundary value problem for solving the hydrodynamic loads on each structural component, the hull is considered as a rigid-body. The second order and higher order terms of the hydro loads on the hull, except for the drag forces induced by viscous effect, and hydroelasticity effects are not included in the approaches discussed in the present paper, but they can be further included. The two assumptions are used to simplify the numerical models for the loads on the structural components. The second assumption can be implemented since the focus of the proposed approach is on capturing the global forces and moments in the structural components.

Details of the approaches for modeling inertial and external loads on each structural component are illustrated as follows.

For each structural component, a body-related coordinate system and a body-fixed coordinate system are established. We denote the origins of the body-related and body-fixed coordinate systems for the structural component i as $O^{r,i}$ and $O^{b,i}$ respectively. When the floating wind turbine is located at its mean position, the body-related and body-fixed coordinate systems for each structural component and the O^f-x^f-y^f-z^f coordinate system are coincident. The body-fixed coordinate system of the structural component i rigidly follows the motion of the corresponding node of the structural component i in the finite element model in the O^g-x^g-y^g-z^g coordinate system. In the O^f-x^f-y^f-z^f coordinate system, the motion of the $O^{b,i}$ and the orientation of the body-fixed coordinate system are described by $\boldsymbol{\eta}^i(t) = [\eta_1^i, \eta_2^i, \eta_3^i, \eta_4^i, \eta_5^i, \eta_6^i]^T$. η_4^i, η_5^i and η_6^i are three Euler angles about x^f, y^f and z^f axis.

The gravity loads of the structural component i can be modeled as constant force acting on the centre of gravity of the structural component i in the body-fixed coordinate system of the structural component i and pointing to the negative direction of the vertical axis of the global coordinate system. Inertial loads of and viscous loads on the structural component i can be calculated in the body-fixed coordinate system. A body mass matrix of each structural component with respect to the origin of the corresponding body-fixed coordinate system can be specified. The viscous loads can be accounted for by the drag term of the Morison formula.

The resultants of the first order radiation and wave excitation loads on the structural component i are represented by $\boldsymbol{L}^t_{external,i}$, see Eq. (1). $\boldsymbol{L}^t_{external,i}$ is described in the body-related coordinate system of the structural component i and acting on the $O^{r,i}$.

$$\boldsymbol{L}^t_{external,i} = \boldsymbol{R}_{potential\_wave\_i}(t) - \int_{-\infty}^{+\infty} \boldsymbol{k}_i(t-\tau)\dot{\boldsymbol{\eta}}^i(\tau)d\tau - \boldsymbol{A}_i^{\infty}\ddot{\boldsymbol{\eta}}^i(t) \tag{1}$$

in the $\boldsymbol{L}^t_{external,i}$, $\boldsymbol{R}_{potential\_wave\_i}(t)$ is the resultants of the wave excitation loads on the structural component i obtained by applying inverse Fourier transform on $\boldsymbol{R}_{wave\_i}(\omega)$. $\boldsymbol{R}_{wave\_i}(\omega)$ is frequency dependent first order wave excitation vector for the structural component i. We have $\boldsymbol{R}_{wave\_i}(\omega) = \boldsymbol{H}_{fw\_i}(\omega)*Amp_\omega \cdot Amp_\omega$ is determined by a spectrum of incident waves. For a sinusoidal wave with a given frequency ω, Amp_ω is the amplitude of the sinusoidal wave. $\boldsymbol{H}_{fw\_i}(\omega)$ is first order wave excitation load transfer function for the structural component i. $\boldsymbol{k}_i(t)$ is known as retardation or memory function for the structural component i and determined by $\boldsymbol{A}_i(\omega)$ or $\boldsymbol{B}_i(\omega)$. $\boldsymbol{A}_i^{\infty}$ is $\boldsymbol{A}_i(\omega)$ corresponding to the high-frequency limit. $\boldsymbol{A}_i(\omega)$ and $\boldsymbol{B}_i(\omega)$ are frequency dependent added mass coefficient matrix and potential damping coefficient matrix for the structural component i.

$\boldsymbol{H}_{fw\_i}(\omega)$, $\boldsymbol{A}_i(\omega)$ and $\boldsymbol{B}_i(\omega)$ are obtained by the following steps, 1) solving the boundary value problem in the O^f-x^f-y^f-z^f coordinate system with the rigid-body assumption for the hull, 2) calculating pressure forces on the mean wet surface of the structural component i ($S^0_{wet,i}$) based on the Bernoulli's equation and corresponding velocity potential, 3) integrating the pressure on the wet surface of the component i (on the $S^0_{wet,i}$) using the coordinate system O^f-x^f-y^f-z^f to obtain the integrated forces and moments acting on O^f, and 4) derive the hydrodynamic coefficients based on the corresponding resultant forces and moments on the O^f in the O^f-x^f-y^f-z^f coordinate system. $\boldsymbol{H}_{fw\_i}(\omega)$, $\boldsymbol{A}_i(\omega)$ and $\boldsymbol{B}_i(\omega)$ include hydrodynamic interactions.

$\boldsymbol{R}^r_{r\_i}(t)$ represents the resultant forces and moments of the hydrostatic pressure forces on the outer surface and the atmospheric pressure forces on the inner surface of the structural component i when the structural component is located at the instantaneous position described by $\boldsymbol{\eta}^i(t) = [\eta_1^i, \eta_2^i, \eta_3^i, \eta_4^i, \eta_5^i, \eta_6^i]^T$ in the O^f-x^f-y^f-z^f coordinate system. $\boldsymbol{R}^r_{r\_i}(t)$ is a 6×1 vector, acting on $O^{r,i}$ and described in the body-related coordinate system.

Neglecting the second order and higher order terms, the expression of the $\boldsymbol{R}^r_{r\_i}(t)$ is derived as:

$$\boldsymbol{R}^{r}_{r\_i}(t) = \boldsymbol{F}_{c_i} + (-1)*\boldsymbol{C}_i\boldsymbol{\eta}^{i}(t) \tag{2}$$

$\boldsymbol{F}_{ci}$ is a 6×1 vector. $\boldsymbol{C}_i$ is a 6 × 6 matrix with real coefficients. The expressions of $\boldsymbol{F}_{ci}$ and $\boldsymbol{C}_i\boldsymbol{\eta}^{i}(t)$ are available in Eqs. (3)–(8).

The coefficients in the $\boldsymbol{C}_i$ and $\boldsymbol{F}_{ci}$ are expressed by parameters that are defined in the O^f-x^f-y^f-z^f coordinate system with respect to the mean wet surface whereas $\boldsymbol{R}^{r}_{r\_i}(t)$ represents forces and moments acting on $O^{r,i}$ in the body-related coordinate system. We assume that the mean outer wet surface of the structural component i and the corresponding inner surface are identical and are denoted as $S^0_{wet,i}$ in the O^f-x^f-y^f-z^f coordinate system. s_0 is a point on the wet surface of the hull. The normal vector and position vector of s_0 at the mean position are denoted as $\boldsymbol{n}_0 = [n_1,n_2,n_3]^T$ and $\boldsymbol{v}_0 = [v_1,v_2,v_3]^T$. $\boldsymbol{n}_0$ is pointing away from the fluid field. Hydrostatic pressure on the s_0 ($P^0_{s_0,hydro\_sta}$) is given by applying Bernoulli's equation. P_0 represents the atmosphere pressure at the still water plane. $Z_0 = 0$ since the O^f-x^f-y^f-z^f coordinate system is located at the still water plane. ρ_f is density of sea water, taken as 1.025 tonnes/m^3. g is gravity acceleration, 9.81 m/s^2. We denote the atmospheric pressure inside the hull as $P_{inner,\,atm}$. We assume $P_{inner,\,atm}$ is constantly equal to P_0. $P^0_{s_0,net}$ denotes the net pressure on the s_0 at the mean position. $P^0_{s_0,net}$ is the difference between the hydrostatic pressure on the outer surface of the s_0 and the atmospheric pressure on the inner surface of the s_0.

$$P^0_{s_0,hydro\_sta} = P_0 + \rho_f g Z_0 - \rho_f g v_3 \tag{3}$$

$$P^0_{s_0,net} = P^0_{s_0,hydro\_sta} - P_{inner,\,atm} \tag{4}$$

$$\boldsymbol{F}_{c_i} = \begin{bmatrix} \iint\limits_{S^0_{wet,i}} \begin{bmatrix} n_1 \\ n_2 \\ n_3 \end{bmatrix} P^0_{s_0,net}\,ds \\ \iint\limits_{S^0_{wet,i}} \begin{bmatrix} v_1 \\ v_2 \\ v_3 \end{bmatrix} \times \begin{bmatrix} n_1 \\ n_2 \\ n_3 \end{bmatrix} P^0_{s_0,net}\,ds \end{bmatrix} \tag{5}$$

$$\boldsymbol{C}_i\boldsymbol{\eta}^{i}(t) = \begin{bmatrix} \boldsymbol{D_1} \\ \boldsymbol{D_2} \end{bmatrix} \tag{6}$$

$$\boldsymbol{D_1} = \rho_f g \iint\limits_{S^0_{wet,i}} \begin{bmatrix} n_1 \\ n_2 \\ n_3 \end{bmatrix} \left(\eta^i_3 + \eta^i_4 v_2 - \eta^i_5 v_1\right) ds - \iint\limits_{S^0_{wet,i}} \begin{bmatrix} \eta^i_4 \\ \eta^i_5 \\ \eta^i_6 \end{bmatrix} \times \begin{bmatrix} n_1 \\ n_2 \\ n_3 \end{bmatrix} P^0_{s_0,net}\,ds \tag{7}$$

$$\boldsymbol{D_2} = \rho_f g \iint\limits_{S^0_{wet,i}} \begin{bmatrix} v_1 \\ v_2 \\ v_3 \end{bmatrix} \times \begin{bmatrix} n_1 \\ n_2 \\ n_3 \end{bmatrix} \left(\eta^i_3 + \eta^i_4 v_2 - \eta^i_5 v_1\right) ds - \iint\limits_{S^0_{wet,i}} \begin{bmatrix} 0 \\ 0 \\ \eta^i_3 \end{bmatrix} \times \begin{bmatrix} n_1 \\ n_2 \\ n_3 \end{bmatrix} P^0_{s_0,net}\,ds - \iint\limits_{S^0_{wet,i}} \begin{bmatrix} \eta^i_4 \\ \eta^i_5 \\ \eta^i_6 \end{bmatrix} \times \left(\begin{bmatrix} v_1 \\ v_2 \\ v_3 \end{bmatrix} \times \begin{bmatrix} n_1 \\ n_2 \\ n_3 \end{bmatrix} \right) P^0_{s_0,net}\,ds \tag{8}$$

Flexibility effects of the hull on the hydro loads are not accounted for. The hydrodynamic loads on each structural component are derived from the velocity potential that are obtained by solving the boundary value problems with the assumption that the hull is a rigid-body. The kinematics of different structural components is constrained by the rigid-body assumption. Consequently, the hydrodynamic interaction effects between the structural components are included in the hydrodynamic loads on each structural component. However, the proposed approach may not be able to well model the hydroelasticity effect. Therefore, it is not recommended to be applied on floating structures with relatively large flexibility, for which hydroelasticity effect can be important.

The expressions of $\boldsymbol{L}^{t}_{external,i}$ and $\boldsymbol{R}^{r}_{r\_i}(t)$ can be further modified. For example, additional terms can be included to account for second order and/or higher order hydro loads on each structural component, while the load effects of the ballast fluid can be modeled as pressure forces on the inner surface of each structural component.

3. Verification of the proposed approach

The proposed approach is implemented in Simo/Riflex/Aerodyn [29–32] to calculate global forces and moments of the 5-MW-CSC [15]. The layout of the semi-submersible floater is given in Figs. 5 and 6. The O^g-x^g-y^g-z^g and O^f-x^f-y^f-z^f coordinate systems are established at the mean position of the geometrical centre of the water plane area.

Five numerical models have been developed. Three comparisons, i.e. Comparison A, Comparison B and Comparison C, have been carried out to verify the proposed approach step by step. These numerical models and the comparisons are briefly

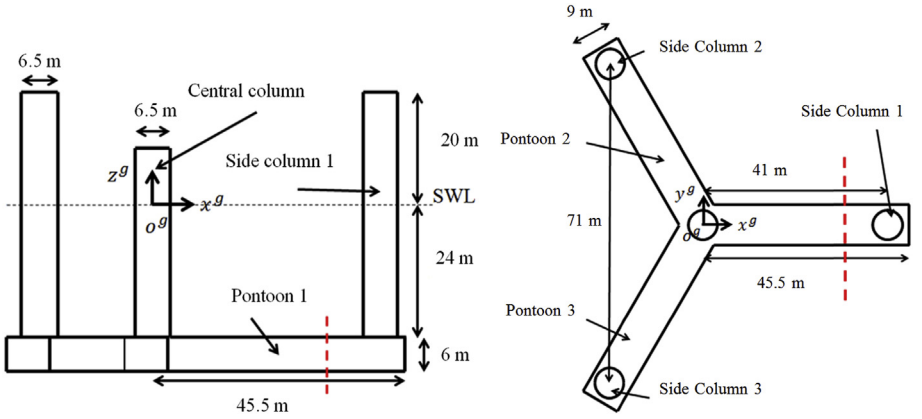

Fig. 5. Side (left) and top (right) views of the semi-submersible hull of 5-MW-CSC.

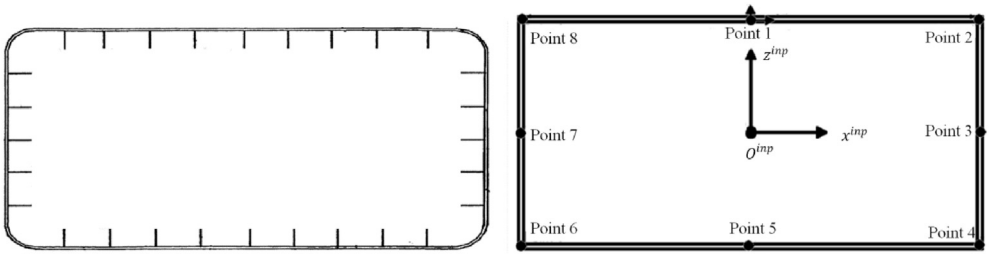

Fig. 6. A realistic cross-section (left) and simplified box-shape cross-section with equivalent thickness (right).

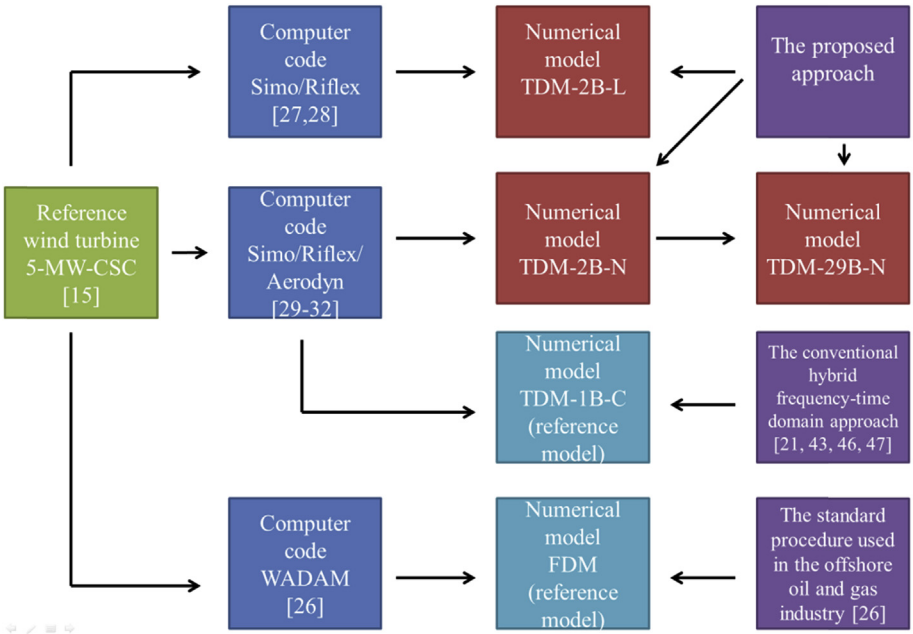

Fig. 7. Numerical models.

explained below and illustrated in Figs. 7 and 8, respectively. Detailed descriptions for the numerical models are available in the later part of this paper. A summary of the features of the time-domain models is available in Table 3.

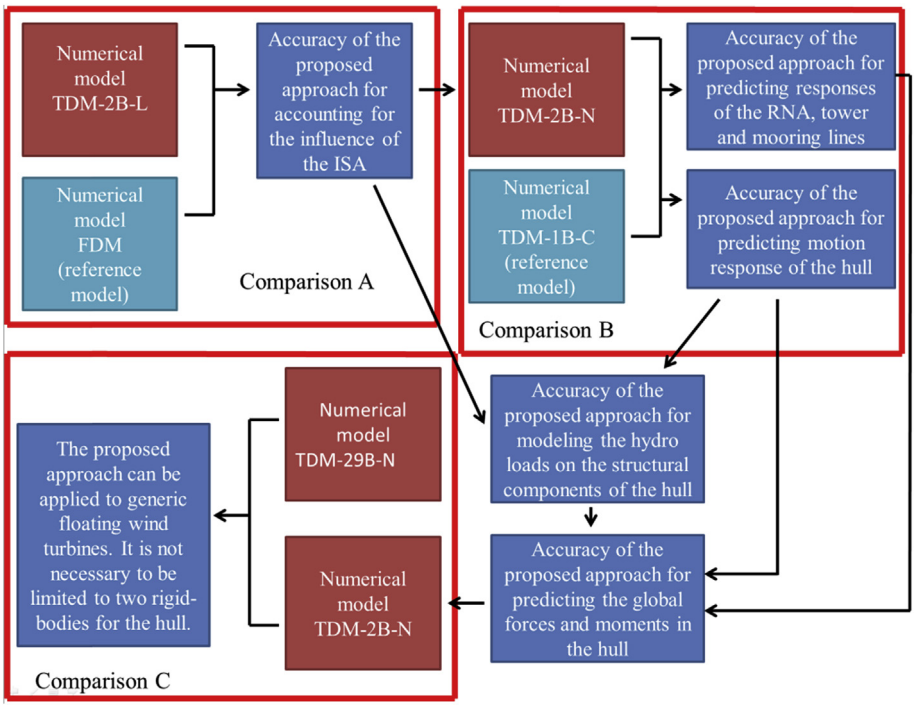

Fig. 8. Verification procedure.

FDM is a frequency-domain model of the 5-MW-CSC developed in WADAM [26] to calculate wave induced global forces and moments by implementing a standard procedure used in the offshore oil and gas industry [26].

TDM-2B-L is a time-domain model of the 5-MW-CSC developed in Simo/Riflex [27,28]. The proposed approach is implemented to calculate wave induced global forces and moments in the cross-section as shown by the dashed line in Fig. 5. Aerodynamic loads are not available in the TDM-2B-L.

TDM-1BC is a time-domain model developed in Simo/Riflex/Aerodyn. Aerodynamic loads on the RNA and tower are appropriately accounted for in the TDM-1BC, while the conventional hybrid frequency-time domain approach is implemented to model the hydro loads on the semi-submersible hull. The modeling approach implemented in the TDM-1BC is considered as the state-of-the-art approach that has been used by researchers, e.g. Refs. [21,43,46,47], to analyze responses of floating wind turbines in wind and waves except for the global forces and moments in the hull since the approach models the hull as one rigid-body with 6 d.o.f.s.

TDM-2BN is an extension of the TDM-1BC. The proposed approach is implemented to calculate global forces and moments in the hull (in the cross-section as shown by the dashed line in Fig. 5). The TDM-1BC and TDM-2BN are identical except for the finite element model of the hull and method for modeling the external and inertial loads on the hull.

TDM-29BN is an extension of the TDM-2BN. The TDM-2BN includes two rigid-bodies for the hull, while, the TDM-29BN includes twenty-nine rigid-bodies for the hull. The TDM-29BN model is developed and compared to the TDM-2BN model in order to show that the proposed method can be generalized to a model consisting of any number of structural components. From the practical use point of review, it is convenient to use the TDM-29BN model to obtain the dynamic responses at any critical position of the hull by just one time-domain model. While, using the TDM-2BN approach, many different numerical models need to be built and analyzed.

It is expected that the time-domain model TDM-2BN can calculate the global forces and moments in the cross-section as shown by the dashed line in Fig. 5 while the time-domain model TDM-29BN can calculate the global forces and moments in the same cross-section and the other twenty-seven cross-sections.

As far as the authors know, there is no published experimental data for the global forces and moments in the hull of floating wind turbines in wind and waves. In addition, the state-of-the-art time-domain computer codes cannot accurately calculate the global forces and moments in the hull [22].

The accuracy of the calculated responses is related to two modeling issues: 1) whether or not the computer codes can accurately calculate the wind and waves induced external and inertial loads on the floating wind turbines and map the loads to the generated finite element models of the floating wind turbines; and 2) whether or not the finite element models generated in the computer codes can accurately represent the global stiffness of the floating wind turbines and calculate the structural responses for given loads. These two features are coupled.

The hull of the 5-MW-CSC is a statically determinate structure. For a statically determinate structure, in general, the accuracy of the responses in the structure is purely determined by the accuracy of the external loads acting on the structural components, like aerodynamic loads on the blades and the tower and hydrodynamic loads on the floater and mooring lines and the inertial loads.

In linear theory, hydrodynamic and hydrostatic loads on structural components of the hull are determined by two issues. We denote these issues as ISA and ISB respectively.

ISA: The configuration and shape of the mean wet surfaces of the structural components.

ISB: The motion responses of the structural components.

The accuracy of the global forces and moments in the hull calculated by the TDM-2BN is indicated by the results of Comparison A and Comparison B. Comparison A focuses on verifying that the influence of the ISA on the hydro loads on the structural components can be accurately modeled in finite element codes which implement the proposed approach. Comparison B focuses on verifying that finite element codes which implement the proposed approach can accurately predict the motion responses of the structural components and responses of the RNA, tower and mooring lines of the reference semi-submersible wind turbine in wind and waves. Comparison C is carried out, to some extent, to address that the proposed approach can be applied to generic floating wind turbines, for which the hull may need to be modeled by any number of structural components. The proposed approach is not necessarily limited to two rigid-bodies for the hull. Due to the limitation of the proposed approach, we do not account for the hydroelasticity effect in the comparisons discussed in the present paper.

In Comparison A, the FDM is used as a reference model for the transfer functions of wave to global forces and moments in the hull. While the transfer functions can also be derived from structural responses of the hull calculated by carrying out regular and/or irregular wave analysis in time-domain numerical models that implement the proposed approach, e.g. TDM-2B-L, TDM-2BN and TDM-29BN. The FDM is a linear system and does not account for non-linear effects on the global forces and moments, while TDM-2B-L is developed to be, as much as possible, a linear system and equivalent to the FDM. The agreement in the transfer functions calculated in the FDM and TDM-2B-L is expected to be good if the proposed approach accurately models the hydro pressure forces on the structural components of the hull and maps the forces on the finite element model of the hull.

TDM-2B-L models the 5-MW-CSC as two structural components connected by three artificial beam elements. Aerodynamic loads are not accounted for in the TDM-2B-L. In contrast, aerodynamic loads are accounted for in the TDM-2BN while the TDM-2BN models the hull of the 5-MW-CSC as two structural components connected by three artificial beam elements and the mooring lines, tower and blades as beam elements. The mean wet surfaces of the two structural components of the TDM-2B-L are identical to the mean wet surfaces of the two structural components of the TDM-2BN correspondingly and respectively. Consequently, if the influence of the ISA on the hydro loads on the structural components can be accurately modeled in TDM-2B-L, the influence can be accurately modeled in the TDM-2BN.

The motions of the hull and responses of the RNA, tower and mooring lines predicted by TDM-2BN and TDM-1BC are compared in Comparison B. TDM-1BC is used as a reference model except for the global forces and moments in the hull. TDM-1BC and TDM-2BN are identical except for the finite element model of the hull and method for modeling the external and inertial loads on the hull. Therefore, agreement in the compared responses is expected to be good.

Since the hull of the 5-MW-CSC is a statically determinate structure, it is expected that the global structural stiffness of the hull does not affect the global forces and moments in the structural components of the hull except for the inertia loads and hydro loads induced by the flexible modes of the hull. The global structural stiffness of the hull is determined by properties of the equivalent cross-sections of the pontoons and columns and material properties, e.g. Young's modulus and modulus of rigidity. In Comparison C, artificial material properties are implemented to make the global structural stiffness of the hull of the TDM-29BN to be of the same magnitude as the one of the TDM-2BN. Consequently, the global forces and moments calculated by the TDM-2BN and TDM-29BN are expected to be identical. Research on the importance of the influence of the inertia loads and hydro loads induced by the flexible modes of the hull is interesting and will be investigated in future.

3.1. FDM

The FDM is a frequency-domain model developed in WADAM [26] to calculate wave induced global forces and moments in a cross-section as shown by the dashed line in Fig. 5. Only wave loads are considered here. A realistic cross-section of the pontoon of the hull may be composed of stiffened plates, stiffeners and girders. As shown in Fig. 6, in global analysis, the realistic cross-section can be simplified as a box-shape cross-section with equivalent thickness. The mean position of the geometrical center of the box-shape cross-section in the O^f-x^f-y^f-z^f coordinate system is (31.5, 0, −27). The cross-section divides the semi-submersible wind turbine into two parts: “Part A” and “Part B”. The wind turbine is included in the “Part B”. The global forces and moments in the cross-section are derived based on the fact that the global forces and moments in the cross-section and inertial and external loads on the “Part A” (as well as on Part B) must be in equilibrium. The standard procedure used in the offshore oil and gas industry [26] is implemented in WADAM to calculate the inertial and external loads on the “Part A”.

The inertial loads on the “Part A” are determined by the mass and acceleration of the “Part A”. Motion equations are generated and solved in frequency domain to derive the acceleration. In the motion equations, the RNA, tower and hull are modeled as a single rigid-body with 6 d.o.f.s. Structural flexibility of the floating wind turbine is neglected. The mooring lines are not included in the rigid-body formulation. Instead, a 6×6 restoring stiffness matrix ($C_{mooring}$) is introduced in the motion

equations to represent the restoring effect of the mooring lines on the motions. Hydrodynamic coefficients used in the motion equations are calculated by solving the potential-flow boundary value problem with the rigid-body assumption. The motion equations do not include viscous effect. The external loads on the "Part A" are composed of the first order hydrodynamic loads and the fluctuations of hydrostatic pressure forces and gravity loads.

$$C_{mooring} = \begin{bmatrix} 114\ kN/m & 0 & 0 & 0 & -2052\ KN & 0 \\ 0 & 114\ kN/m & 0 & 2052\ KN & 0 & 0 \\ 0 & 0 & 0 & 0 & 0 & 0 \\ 0 & 2052\ KN & 0 & 149669\ kN*m & 0 & 0 \\ -2052\ KN & 0 & 0 & 0 & 149669\ kN*m & 0 \\ 0 & 0 & 0 & 0 & 0 & 204628\ kN*m \end{bmatrix} \quad (9)$$

3.2. TDM-2B-L

The TDM-2B-L is a time-domain model developed in Simo/Riflex [27,28] and implements the proposed approach. We intend to make it be, as much as possible, equivalent to the FDM. That means, in the TDM-2B-L, the "Part A" and "Part B" are modeled as two rigid-bodies. Each rigid-body has 6 d.o.f.s. The origins of the body-fixed and body-related coordinate systems for the two rigid-bodies are denoted as $O^{b,PA}$ and $O^{r,PA}$ and $O^{b,PB}$ and $O^{r,PB}$ respectively. When the floating wind turbine is located at its mean position, the body-fixed and body-related coordinate systems are coincident to the O^f-x^f-y^f-z^f coordinate system. The positions and orientations of the $O^{b,PA}$ and $O^{b,PB}$ are described by $\boldsymbol{\eta}^{PA}(t)$ and $\boldsymbol{\eta}^{PB}(t)$ in the O^f-x^f-y^f-z^f coordinate system. In the frequency-domain model, the global forces and moments in the cross-section are derived from the equilibrium between the relevant external and inertial loads and the global forces and moments. However, to calculate the global forces and moments in a straight-forward manner in Simo/Riflex, we must have a finite element model. Consequently, the two rigid-bodies are connected by three artificial beam elements. The mean positions of the end nodes of the artificial beams in the O^f-x^f-y^f-z^f coordinate system are tabulated in Table 1. Each end node rigidly follows the motions of its corresponding rigid-body ($\boldsymbol{\eta}^{PA}(t)$ or $\boldsymbol{\eta}^{PB}(t)$). The artificial beam elements are massless. There are no external loads on the artificial beam elements. Each artificial beam element only has axial and torsional stiffness. Artificial Young's modulus and modulus of rigidity are specified to make the artificial beams be stiff. For each beam element, the product of the Young's modulus and cross-section area is specified as 10^9 kN, while, the product of the torsional rigidity and modulus of rigidity are specified as 10^9 kNm^2/rad. The proposed approach is implemented to calculate the first order hydrodynamic loads, gravity and hydrostatic pressure forces on the "Part A" and "Part B" and map the loads on the end nodes of the artificial beam elements. Viscous loads on the hull are not included. The mooring lines induced forces and moments on the floating wind turbine are accounted for by $(-1)^*C_{mooring}^*\boldsymbol{\eta}^{PB}(t)$, which are acting on $O^{r,PB}$ and described in the body-related coordinate system of the rigid-body that corresponds to the "Part B".

3.3. TDM-1BC

The TDM-1BC is a time-domain model developed in Simo/Riflex/Aerodyn. The time-domain model implements the conventional hybrid frequency-time domain approach. The hull is modeled as a rigid-body with 6 d.o.f.s in Simo. The conventional hybrid frequency-time domain approach is used to account for the first order wave excitation and radiation loads on the hull. The blades, shaft of the drive train inside the nacelle, tower and mooring lines are modeled as beam elements in Riflex. The motions of the lower end node of the tower and the upper nodes of the mooring lines rigidly follow the motions of the hull. The hub and nacelle are modeled as rigid mass points attached on the shaft and top of the tower. Aerodynamic loads on the blades and tower are calculated in Aerodyn [32]. A dll file [31] is used to account for the effect of pitch control on aerodynamic loads on the three blades and the effect of the generator inside the nacelle on the power production and generator torque. The torque of the generator is calculated by the dll file based on the rotational speed of the shaft. The shaft is rotational about its longitudinal axis. The rotational d.o.f. is achieved by applying a flex joint [28] on the beam element of the shaft. The blades are connected to the tower through the shaft. Loads on the blades, hub, shaft and generator torque are transferred through the flex joint to the beam element of the tower. Hydrodynamic loads on the mooring lines are accounted for by the Morison formula. The drag term of the Morison formula is used to account for the viscous loads on the hull. The non-dimensional drag coefficients (C_d) are specified in DNV [33]. C_d for the width and height of the pontoons of the 5-MW-CSC is 1.95. C_d for the central column is 0.8. C_d for the side columns is 0.64. The work-flow chart is available in Fig. 1.

Table 1
Positions of end nodes of three artificial beams in the body-fixed coordinate system (Units in meter).

	End 1	End 2
Artificial beam 1	(31.4,0,−27)	(31.6,0,−27)
Artificial beam 2	(31.5,-0.1,−27)	(31.5,0.1,−27)
Artificial beam 3	(31.5,0,−27.1)	(31.5,0,−26.9)

3.4. TDM-2BN

The TDM-1BC and TDM-2BN are identical except for the finite element model of the hull and method for modeling the external and inertial loads on the hull. The cross-section, as shown by the dashed line in Fig. 5, discretizes the hull into two components. The two components of the hull are modeled as two rigid-bodies: "Body1" and "Body2". The wind turbine is mounted on the "Body 2". Each rigid-body has 6 d.o.f.s. The origins of the body-fixed and body-related coordinate systems for the "Body1" and "Body2" are denoted as $O^{b,B1}$ and $O^{r,B1}$ and $O^{b,B2}$ and $O^{r,B2}$ respectively. When the floating wind turbine is located at its mean position, the body-fixed and body-related coordinate systems are coincident to the O^f-x^f-y^f-z^f coordinate system. The positions and orientations of the $O^{b,B1}$ and $O^{b,B2}$ are described by $\boldsymbol{\eta}^{B1}(t)$ and $\boldsymbol{\eta}^{B2}(t)$ in the O^f-x^f-y^f-z^f coordinate system. The two rigid-bodies are connected by the artificial beam elements used in the TDM-2B-L. Each end node of the artificial beam element rigidly follows the motions of its corresponding rigid-body ($\boldsymbol{\eta}^{B1}(t)$ or $\boldsymbol{\eta}^{B2}(t)$). The proposed approach is implemented to calculate the first order hydrodynamic loads, gravity and hydrostatic pressure forces on the "Body1" and "Body2" and map the loads on the end nodes of the artificial beam elements. The drag term of the Morison formula is used to account for the viscous loads on the hull. The non-dimensional drag coefficients used in TDM-2B-L and TDM-2BN are identical. The work-flow chart is available in Fig. 3.

3.5. TDM-29BN

The TDM-29BN is an extension of the TDM-2BN. Numerical models for the RNA, tower and mooring lines of the TDM-2BN and TDM-29BN are identical. In the TDM-29BN, we consider that the hull is composed of twenty-nine structural components. For example, the blue colored parts in Fig. 9 are the structural components named "ICP_S1" and "SP3_2" respectively. Each structural component corresponds to a reference node (the brown colored circle). Each reference point represents 6 d.o.f.s of the corresponding structural component. The reference points are connected by beam elements that represent the flexibility of the hull. The beam elements are massless and there are no external loads on the beam elements. The viscous drag is accounted for by the drag term of the Morison formula and being integrated and transferred to the corresponding reference nodes. The end nodes of beam elements rigidly follow the motions of the corresponding reference node. In the 5-MW-CSC, there are four interfaces between the columns and pontoons. The ICP_S1 represents an interface between the side column 1 and the pontoon 1. For the TDM-29BN, the stiffness of the interfaces is not modeled since the interfaces are modeled as rigid-bodies. The stiffness of the beam elements are determined by properties of the equivalent cross-sections of the pontoons and columns and material properties, e.g. Young's modulus and modulus of rigidity. In the Comparison C, artificial material properties are implemented to make the global structural stiffness of the hull of the TDM-29BN be in the same level as the one of the TDM-2BN. The specified stiffness properties of the beam elements are tabulated in Table 2. EA_g represents the product of the Young's modulus and cross-section area. EI_g represents the product of the Young's modulus and the second moment of the area of the cross-section. GJ_g represents the product of the torsional rigidity and modulus of rigidity. The work-flow chart is available in Fig. 3.

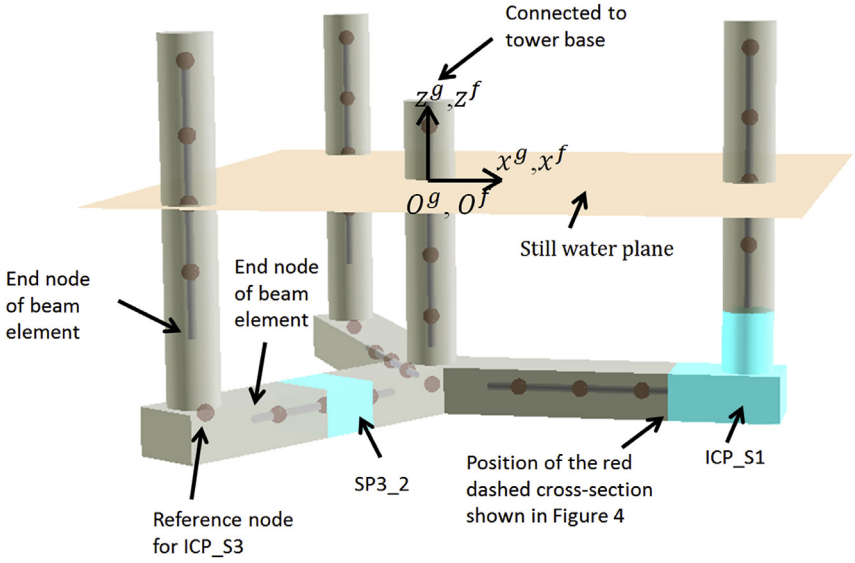

Fig. 9. The finite element model of the hull with twenty-nine bodies.

Table 2
Specified stiffness properties of the beam elements used in TDM-29BN.

	EA_g [kN]	EI_g [kNm^2]	GJ_g [kNm^2/rad]
Column	$1.29*10^{10}$	$6.79*10^{10}$	$5.11*10^{10}$
Pontoon	$1.89*10^{10}$	$6.27*10^{10}$	$2.00*10^{10}$

4. Results and discussions

4.1. Comparison A

F_x, F_y, F_z, M_x, M_y, and M_z denote the wave induced global forces and moments in the cross-section shown by the dashed line in Figs. 5 and 6. The global forces and moments are acting on the origin of the O^{inp}-x^{inp}-y^{inp}-z^{inp} coordinate system and described in the O^{inp}-x^{inp}-y^{inp}-z^{inp} coordinate system. The O^{inp}-x^{inp}-y^{inp}-z^{inp} coordinate system is a body-fixed coordinate system. When the 5-MW-CSC is located at its mean position, the body-fixed coordinate system is coincident to the O^f-x^f-y^f-z^f coordinate system except that the origin of the body-fixed coordinate system is located at the geometrical center of the cross-section which is (31.5, 0, -27) in the O^f-x^f-y^f-z^f coordinate system.

For a given point on the cross-section, axial stress (σ_x) and shear stress (τ) are calculated by Eqs. (10) and (11).

$$\sigma_x = \frac{F_x}{A} + \frac{M_y}{w_{y\_inp}} + \frac{M_z}{w_{z\_inp}} \tag{10}$$

$$\tau = \frac{M_x}{2A_0 t_c} + \frac{F_y S_{z\_inp}}{I_{z\_inp} t_c} + \frac{F_z S_{y\_inp}}{I_{y\_inp} t_c} \tag{11}$$

A is the area of the cross-section. w_{y_inp} and w_{z_inp} are the section moduli corresponding to the y_inp and z_inp axes and the position of the point on the cross-section. A_0 is the circumscribed area of the cross-section. t_c is the equivalent thickness of the cross-section. S_{y_inp} and S_{z_inp} are static moments corresponding to the y_inp and z_inp axes and the position of the point on the cross-section. I_{y_inp} and I_{z_inp} are the second moments of area of the cross-section.

For the TDM-2B-L, transfer function moduli for wave induced global forces and moments and axial and shear stresses can be obtained by carrying out irregular wave analysis or regular wave analysis.

Regular wave analysis can directly give the moduli and phase angles of the transfer functions; however, the phase angles are very sensitive to numerical issues. The transfer functions corresponding to 19 different wave directions and 58 different frequencies are calculated. The wave direction varies from 0° to 180° with 10-degree intervals. The frequencies are distributed in the range from 0.3 rad/s to 2.2 rad/s. The amplitude of each regular wave is specified as 0.1 m.

Alternatively, transfer function moduli can be derived from the spectral densities of the incident waves and global forces and moments. For each wave direction, a 10-hour realization of wave elevation is generated from a white noise spectrum. The frequency range of the spectrum is from 0.3 rad/s to 2.2 rad/s. Significant wave height of the spectrum is specified as 1.233 m ($H_s = 4\sqrt{m_0}$, m_0 denotes the variance-area under the spectral density function). The wave induced motions and global forces and moments are calculated by the TDM-2B-L. The spectral densities are obtained by applying inverse Fourier transform, with a fixed smoothing parameter, of the autocorrelation function of the incident wave and global forces and moments.

The relative difference (R_b) in the obtained transfer function is employed to show the difference in two groups of data. R_b is used to address the relative difference with respect to the corresponding maximum value in the entire wave frequency range (from 0.35 rad/s to 2 rad/s). For example,$e(\omega) = \{e(\omega_1), e(\omega_2),\ldots e(\omega_i),\ldots\}$ and $f(\omega) = \{f(\omega_1), f(\omega_2),\ldots f(\omega_i),\ldots\}$ represent transfer function moduli for wave induced axial force ($|H_{Fx}|$). The transfer function moduli are calculated by carrying out irregular wave analysis and regular wave analysis respectively. ω_i is a given frequency.

$$R_b(\omega_i) = |e(\omega_i) - f(\omega_i)| / \max\{e(\omega),\ f(\omega)\} \times 100\% \tag{12}$$

Transfer function moduli for wave induced global forces and moments and axial and shear stresses obtained by carrying out regular and irregular wave analysis in the TDM-2B-L are compared. The agreement is good. The largest R_b for the transfer function moduli for axial and shear stresses is less than 6%. For most of the transfer function moduli, R_b is less than 3%. Therefore, for the TDM-2B-L, in the following, the transfer function moduli are obtained by carrying out irregular wave analysis.

The transfer function moduli given by the FDM and TDM-2B-L are compared. Some selected results are shown in the present paper. Note that the trend of the transfer function moduli for the sectional forces and moments are not necessary to be the same as that of the total integrated wave excitation loads or motions. The sectional forces and moments are resultants of the difference between the effects of these two on the structure.

The main observations are discussed as follows:

The agreement in transfer function moduli for the global forces and moments and stresses given by the FDM and TDM-2B-L is very good. The relative differences (R_b) vary with respect to the wave frequency and wave direction. In general, peak values of R_b may appear at frequencies nearby troughs of the transfer function modulus curves. However, the effect of the peak values of R_b on the accuracy of the global forces and moments calculated by the TDM-2B-L is very limited. This is because, in the frequency range from 0.35 rad/s to 2 rad/s, for most of the transfer function moduli, R_b is less than 2.5%. The maximum value of R_b for the transfer function moduli for stresses and for global forces and moments is no more than 8% and 5.9% respectively. Two examples are available in Figs. 10 and 11. Position of the points on the cross-section is shown in Fig. 6.

The difference between the FDM and TDM-2B-L is induced by: 1) inherent difference between frequency-domain and time-domain models; 2) accuracy limitation for the numerical solver and other numerical issues.

Detailed discussions are as follows:

- Transfer function moduli for the global forces and moments and stresses subjected to the white noise irregular wave analysis with $H_s = 1.233$ m and $H_s = 12.33$ m are compared. For wave directions, where yaw motion is very small due to the shape of the wet surface of the hull, i.e. 0-degree-wave, 60-degree-wave and 120-degree-wave, R_b for the transfer function moduli is close to zero and indicates that the difference is negligible. In the rest wave directions, the difference is significant. In the frequency range from 0.85 rad/s to 2 rad/s, R_b for the transfer function moduli for the stresses can be up to 28% (in the area around 1.85 rad/s). In the frequency range from 0.35 rad/s to 0.85 rad/s, R_b for the transfer function moduli for the stresses is less than 5%. An example is shown in Fig. 12.
- Transfer function moduli for the responses are calculated by the TDM-2B-L based on two groups of random seed. R_b for the transfer function moduli for the stresses is in the range of 0%–2.2%. The difference may be induced by stochastic uncertainties, non-linear effect and/or numerical errors.
- The mooring lines, tower and blades are flexible slender structures, while the hull and shaft are very stiff. For a large volume structure, such as the 5-MW-CSC, the integrated hydrodynamic loads on the hull can be much larger than the integrated aerodynamic loads on the blades or hydrodynamic loads on the mooring lines. The large variations in the generalized stiffness matrix and external load vectors of the finite element model of the floating wind turbine may, numerically, result in an accuracy limitation and/or numerical errors.
- In Simo/Riflex, global shear forces in the beam elements are calculated by the Euler–Bernoulli beam theory. If the three artificial beam elements of the TDM-2B-L are replaced by a very short (0.1 m) beam element with very large axial, torsional and bending stiffness, the shear forces calculated by the TDM-2B-L are strange and wrong until the bending stiffness of the beam element is reduced and/or the length of the beam element is increased.
- The TDM-2B-L does not have viscous damping. Therefore, very limited wave energy at the resonant frequencies can result in very large resonant motions. The amplitude of the resonant motions could be much larger than the amplitude of the motions in the wave frequency range. The very large resonant motions can introduce strong numerical noise on the realizations of the motions in the wave frequency range. Therefore, the lower limit of the frequency range of the white noise spectrum used in the irregular wave analysis is specified as 0.3 rad/s to keep the wave energy be away from the resonant frequencies, avoid very large resonant motions and limit the numerical noise. Alternatively, the numerical noise can be moderated by introducing viscous effect into the numerical model.

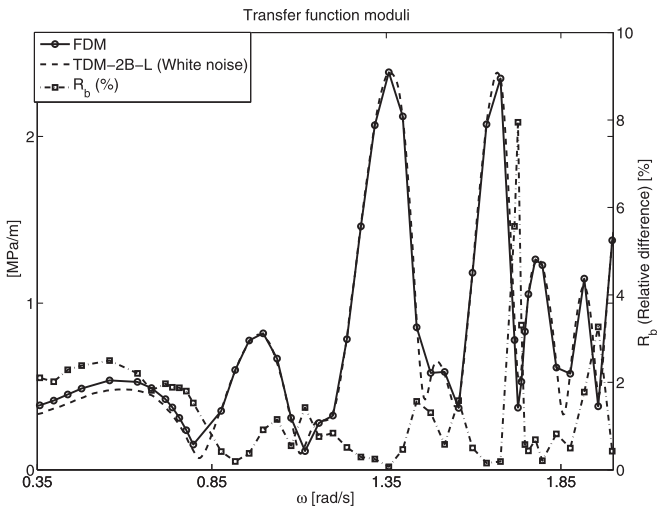

Fig. 10. Comparison of transfer function modulus curves for the axial stress at the point 6 given by the FDM and TDM-2B-L subjected to 120-degree-wave.

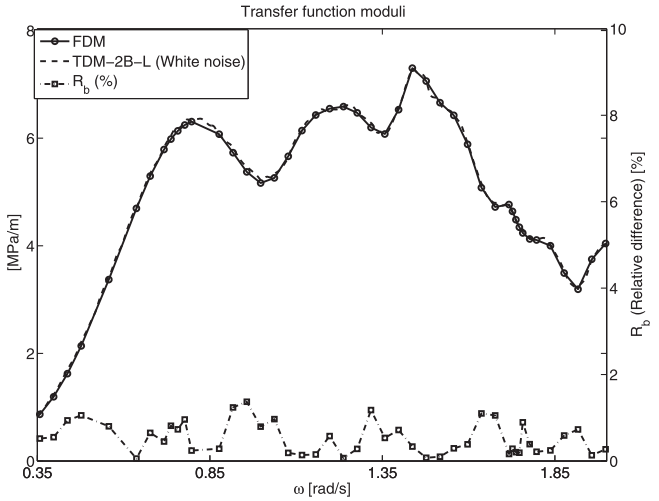

Fig. 11. Comparison of transfer function modulus curves for the axial stress at the point 1 given by the FDM and TDM-2B-L subjected to 10-degree-wave.

- In the TDM-2B-L, the first order wave excitation loads on the hull are generated from the corresponding spectral densities of the wave excitation loads. "WETFF59" and "WETFF199" represent wave to wave excitation load transfer functions that correspond to a set of 59 selected frequencies and a set of 199 selected frequencies respectively. If the TDM-2B-L use the "WETFF59" and is subjected to 80-degree-wave, 90-degree-wave or 100-degree-wave, the TDM-2B-L will give strange results in the transfer functions for the global forces and moments. The strange results will disappear if the "WETFF59" is replaced by "WETFF199". Fig. 13 shows the transfer function modulus curves for the global lateral shear force (F_y) given by the FDM and TDM-2B-L, which use the "WETFF59" and is subjected to 90-degree-wave, as an example. Compare to the FDM, the TDM-2B-L gives strange transfer function moduli ("an impulse") in the frequency range from 0.79 rad/s to 0.89 rad/s. We can observe similar strange results in the spectral densities for the global forces and moments given by the TDM-2B-L that implements the "WETFF59" rather than the "WETFF199". Fig. 14 shows the spectral densities for the global lateral shear force (F_y) given by the TDM-2B-L that implements the "WETFF59" and "WETFF199" respectively. The circles and squares on the curves represent the set of the 59 selected frequencies and set of the 199 selected frequencies respectively. The spectral densities are generated based on the same smoothing factor for the inverse Fourier transform. The realizations of the global forces and moments are calculated based on the same realization of the wave elevation. In the frequency range from 0.79 rad/s to 0.89 rad/s, the set of the 59 selected frequencies for the "WETFF59" has two frequencies (0.797 rad/s and 0.877 rad/s). These two frequencies are nearby the boundary of the range and sufficient to represent the wave excitation transfer functions in the range. The set of the 199 selected frequencies for the "WETFF199" has 12 frequencies uniformly distributed in the range. The "WETFF59" agree with the "WETFF199", while, the "WETFF199" are smoother since the "WETFF199" include more frequencies. Fig. 15 shows the transfer function curves for the lateral wave excitation force on the "PartA" in 90-degree-wave, as an example. We do not observe similar strange results in the "WETFF59" and "WETFF199". We can conclude that the strange results are related to the selected frequencies for the wave excitation transfer functions. However, the reason is not clear yet. In this paper, the numerical models, which implement the proposed method, utilize the "WETFF199". In general, a refined frequency resolution should be considered when using irregular wave analysis to obtain the transfer function.

4.2. Comparison B and comparison C

Ten combined wind and wave conditions are selected from a site in northern North Sea [34] and tabulated in Table 4. The combined wind and wave conditions are composed of five different mean wind speeds covering the below rated, at rated, above rated and parked wind speed and two wave directions. In addition, we also looked at wave only conditions by removing the winds from the combined conditions. For each condition, one 1-hour time-domain simulation is carried out in the TDM-1BC, TDM-2BN and TDM-29BN respectively. Identical random seeds are used to eliminate stochastic uncertainties. Responses, i.e. the pitch angle of each blade, azimuth angle and rotational speed of the rotor, aerodynamic forces and moments on the rotor, torque on the rotational shaft of the drive train, generator torque, generated power, global forces and moments in a given cross section of the tower, global rigid-body motions of the hull and mooring line tension at the top end (fairlead) of each mooring line, are calculated and compared. Definition of the directions of wind and waves is available in Fig. 16.

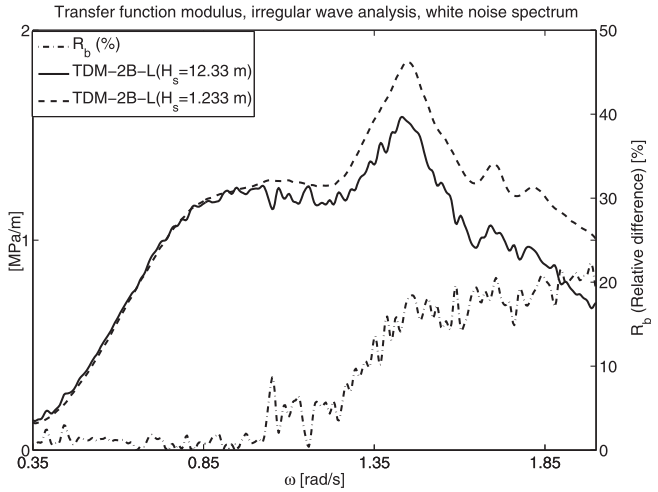

Fig. 12. Comparison of transfer function modulus curves for the axial stress at the point 3 given by the TDM-2B-L subjected to 80-degree-wave and different significant wave heights.

Results and discussions with respect to the Comparison B are given as follows:

The responses of the TDM-1BC and TDM-2BN subjected to the wave only conditions are firstly compared. We find that the responses are identical to each other (the difference is negligible). Part of the realization of the fore-aft bending moment at the tower base, in EC02000 (wave only), is given as an example, see Fig. 17.

Then, the responses of the TDM-1BC and TDM-2BN subjected to the combined wind and wave conditions are compared. When the relative wind speed at the hub is below the rated speed, the generator torque and rotational speed of the rotor will be adjusted by the controller to optimize the power generation. A slightly numerical difference in the TDM-1BC and TDM-2BN can result in slightly differences (phase shift) in the azimuth angle and rotational speed of the rotor. The differences will be accumulated with development of simulation time and result in developing differences in the aerodynamic loads on the rotor, global forces and moments at the tower base and mooring line tensions at the fairleads. As shown in Figs. 18 and 19, the realizations of the azimuth angle of the TDM-1BC and TDM-2BN are identical at the beginning but the phase shift is accumulated with the development of the simulation time. The differences induced by the phase shift have very limited effects on the realizations of the rigid-body motions of the hull and spectra of the global forces and moments at the tower base, mooring line tensions and rigid-body motions. Spectral densities of the fore-aft bending moment at the tower base of the TDM-1BC and TDM-2BN are given in Fig. 20 as an example.

For EC04000 and EC04090, the relative wind speed at nacelle is always above the rate speed. Therefore, the generator torque is constant and azimuth angles of TDM-1BC and TDM-2BN are in phase. Very slightly difference exists in the responses, see Fig. 21 as an example. The difference is induced by very slightly numerical difference in pitch actuator control. Identical responses can be obtained if the control model is removed from the TDM-1BC and TDM-2BN. In EC05000 and EC05090, where the wind turbine is parked, identical responses are observed.

Results and discussions with respect to the Comparison C are given as follows:

We compare the responses of the TDM-2BN and TDM-29BN in wave only and in combined wind and wave conditions. Observations of the comparisons of the responses of the RNA, tower and mooring lines of the TDM-2BN and TDM-29BN are similar to the observations of the comparison of the TDM-1BC and TDM-2BN which have been illustrated in above.

Therefore, we focus on discussions with respect to the global forces and moments in the cross-section shown in Fig. 5. As mentioned in above, the global forces and moments in the cross-section (the dashed line) are described in the O^{inp}-x^{inp}-y^{inp}-z^{inp} coordinate system and are denoted as F_x, F_y, F_z, M_x, M_y, and M_z. For each condition, time realizations of the global forces and moments of the TDM-2BN and TDM-29BN are in phase and almost identical. An example is given in Fig. 22.

When the floating wind turbine is located in calm water without wind loads, the global forces and moments in the hull are static and are determined by the gravity and hydrostatic pressures forces on the floating wind turbine. We find the difference in the static loads calculated by the TDM-2BN and TDM-29 and the analytical solution is less than 1%.

Figs. 23 and 24 show the spectral densities of the M_y (bending moment) of the TDM-2BN and TDM-29BN in EC01000, EC02000, EC03000, EC04000 and EC05000. We do not observe any high frequency responses (in the frequency range 2 rad/s to 4 rad/s). The peaks of the density curves in the frequency range 0.5 rad/s to 2 rad/s correspond to the T_p of the wave spectrum, while, in the operational conditions, considerable low-frequency (from 0 rad/s to 0.3 rad/s) components can be observed. The standard deviation of the M_y, for example, in EC03000 with combined wind and waves is 21.4 MN*m, while the standard deviation of the M_y in EC03000 with waves only is 15.2 MN*m. The relative difference is 41%.

In the low frequency range, the global forces and moments in the structural components of the hull are sensitive to fluctuations of the hydrostatic pressure forces on the structural components. This is because: 1) the aerodynamic loads on the

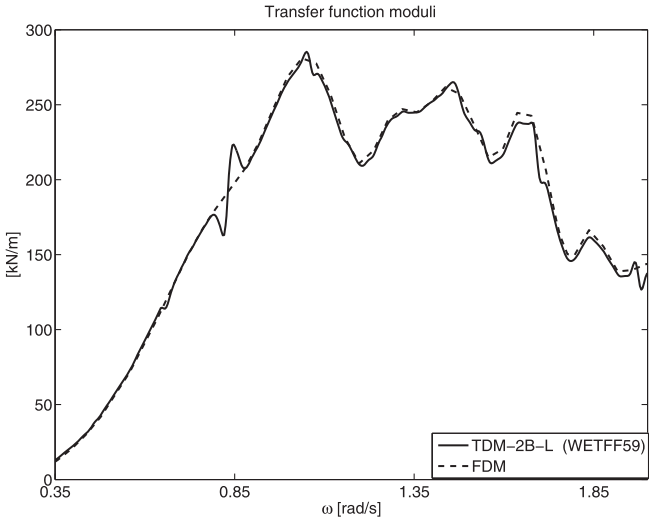

Fig. 13. Comparison of transfer function modulus curves for the global lateral shear force ($\boldsymbol{F_y}$) given by the FDM and TDM-2B-L (based on the "WETFF59"), subjected to 90-degree-wave.

RNA and tower can excite significant rotational motions (e.g. roll and pitch) in particular in the low frequency range comparing to the motions excited by the wave excitation loads on the hull, while the first order terms of the fluctuations of the hydrostatic pressure forces are proportional to the motions; 2) wave excitation loads are expected to be small since wave energy is expected to be very limited (except for swell) in the low-frequency range; and 3) inertia and radiation loads are proportional to the first order derivative (velocity) and second order derivative (acceleration) of the motions and are expected to be small in the low-frequency range.

5. Conclusions

The present paper deals with the development and verification of a time-domain approach that can be easily implemented in various state-of-the-art computer codes to extend their capabilities to analyze global forces and moments in structural components of a generic floater subject to linear and non-linear environmental loads from wind and waves. The global forces and moments in the structural components might be used as inputs of design formulas for structural strength design checks and/or used as boundary conditions in a sub-model finite element analysis to determine structural responses such as stresses, etc.

The proposed approach focuses on the modeling of the inertia and external loads on the hull and the mapping of the loads in the finite element model of the hull. In the proposed approach, floating wind turbines are considered as an assemblage of several structural components. The conventional hybrid frequency-time domain approach is extended to model the external loads on and inertia loads of each structural component. Hydrodynamic loads on each structural component are obtained by integrating the pressure loads that are obtained by solving the linear hydrodynamic problem with the assumption that the hull is a rigid-body. The kinematics of different structural components is constrained by the rigid-body assumption. The proposed approach does not account for hydroelasticity effects. The expressions of the hydro loads on each structural component can be further modified to account for, for example, second order and/or higher order hydro loads on each structural component. Beam elements are used to represent the global stiffness of the structural components but the proposed approach can be further extended to use other finite element models to represent the stiffness of the structural components.

So far, the proposed approach has been implemented in the computer code Simo/Riflex/Aerodyn to analyze global forces and moments in the hull of a semi-submersible wind turbine. Responses calculated by the numerical models that implement the proposed approach and obtained by the reference models are compared step by step. The agreements are very good. Accuracy of the proposed approach needs to be further checked by sensitivity studies and by comparison to the model test data.

In the operational conditions, considerable low-frequency components can be observed in the spectra of the obtained global forces and moments in the pontoons of the reference floating wind turbine. The results indicate that the low-frequency aerodynamic loads, the fluctuations of the hydrostatic pressure forces and the fluctuations of the gravity loads of floating wind turbines are important contributions to the structural responses, in particular, in the low-frequency range. This feature needs to be further investigated by experimental studies.

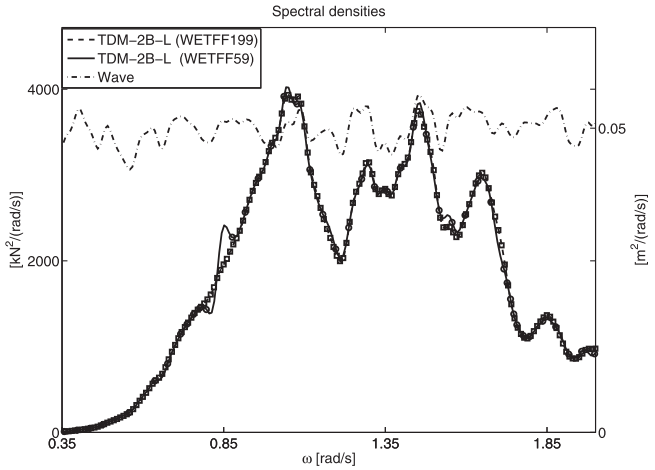

Fig. 14. Spectral densities of the global lateral shear force (F_y) calculated by the TDM-2B-L based on the "WETFF59" and "WETFF199". Wave direction is 90-degree. The circles and squares on the curves represent the set of the 59 selected frequencies and set of the 199 selected frequencies respectively.

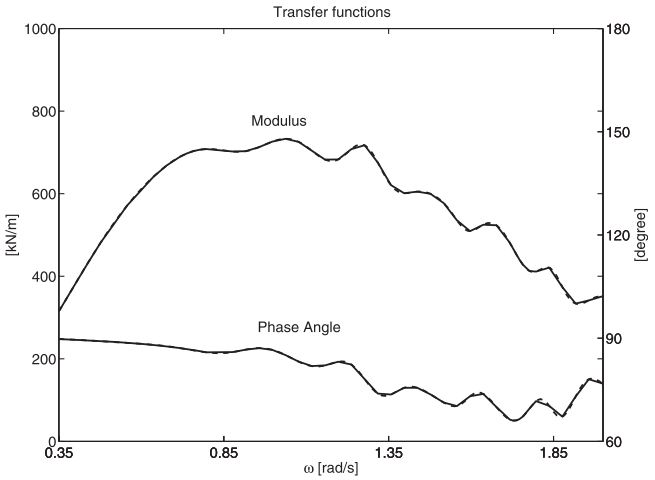

Fig. 15. Moduli and phase angles of transfer functions of wave to lateral wave excitation force on the "PartA", subjected to 90-degree-wave. The solid lines represent the moduli and phase angles corresponding to the set of the 59 selected frequencies. The dashed lines represent the moduli and phase angles corresponding to the set of the 199 selected frequencies.

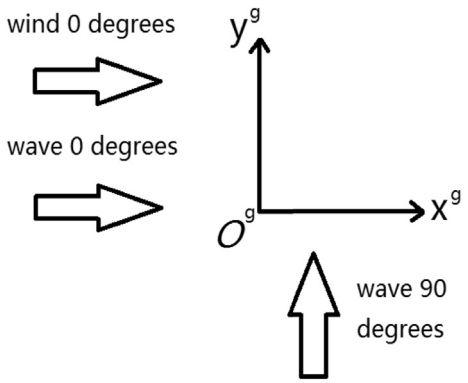

Fig. 16. Definition of the directions of wind and waves.

Table 3
Summary of the features of the time-domain models.

	TDM-2B-L	TDM-1BC	TDM-2BN/TDM-29BN
Mass and structural models			
The hull	The floating wind turbine is divided into two parts: "Part A" and "Part B". The two parts are modeled as two rigid-bodies. Each rigid-body has 6 d.o.f.s. The two rigid-bodies are connected by three artificial beam elements. Integrated mass (corresponding to each rigid-body).	The hull is modeled as one rigid-body with 6 d.o.f.s. Integrated mass.	The hull is discretized as two rigid-bodies: "Body1" and "Body2"/twenty-nine rigid-bodies. Each rigid-body has 6 d.o.f.s. The two rigid-bodies are connected by three artificial beam elements/The twenty-nine rigid-bodies are connected by beam elements. Integrated mass (corresponding to each rigid-body)
Nacelle	Rigid-bodies with integrated mass (Included in the rigid-body for the "Part B").	Mass point attached to tower top	Identical to TDM-1BC
hub		Mass point attached to shaft	
Tower		Flexible bodies	
Blades		Beam elements	
Shaft		Distributed mass	
Mooring lines	The finite element model of the mooring lines is not developed.		
External load model			
The hull	1) Gravity loads 2) Extended hybrid frequency-time domain approach 3)Hydrostatic pressure force 4) Rayleigh damping (the part that is proportional to the structural stiffness) 5) Linearized restoring forces and moments provided by the mooring lines.	1) Gravity loads 2) Conventional hybrid frequency-time domain approach 3) Viscous force (Drag term of the Morison formula) 4) Hydrostatic pressure force	1) Gravity loads 2) Extended hybrid frequency-time domain approach 3) Viscous force (Drag term of the Morison formula. The drag coefficients are identical to TDM-1BC) 4) Hydrostatic pressure force 5) Rayleigh damping (the part that is proportional to the structural stiffness)
Nacelle	1) Gravity loads	1) Gravity loads	Identical to TDM-1BC
hub		2) Rayleigh damping (the part that is proportional to the structural stiffness)	
Tower			
Blades		1) Gravity loads 2) Aerodynamic loads (Aerodyn) 3) Rayleigh damping (the part that is proportional to the structural stiffness)	
Shaft		1)Generator torque	
Mooring lines	None	1) Gravity and Buoyancy loads 2) Morison formula	

Table 4
Environmental conditions.

Environmental conditions	Mean wind speed at nacelle height [m/s]	Turbulence intensity [%]	H_s [m]	T_p [s]	Wave direction [degree]	Note
EC01000	4.9	23	4.6	8	0	Wind turbine in operation; Two-parameter JONSWAP spectrum
EC01090	4.9	23	4.6	8	90	
EC02000	8.0	17	5.2	8	0	
EC02090	8.0	17	5.2	8	90	
EC03000	11.0	15	5.7	8	0	
EC03090	11.0	15	5.7	8	90	
EC04000	16.5	13	6.5	8	0	
EC04090	16.5	13	6.5	8	90	
EC05000	34.6	11.1	8.7	9	0	Wind turbine parked;
EC05090	34.6	11.1	8.7	9	90	Two-parameter JONSWAP spectrum

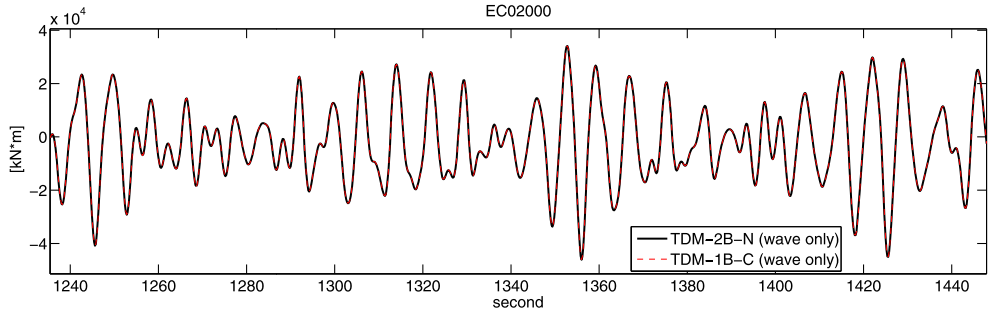

Fig. 17. An example of the time series of the fore-aft bending moment at the tower base of the TDM-1B-C and TDM-2B-N, EC02000 (wave only).

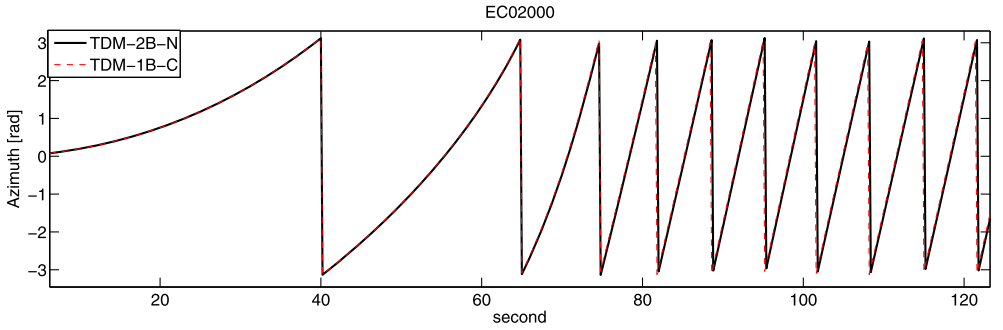

Fig. 18. An example of the time series of the azimuth angle of the TDM-1B-C and TDM-2B-N, EC02000.

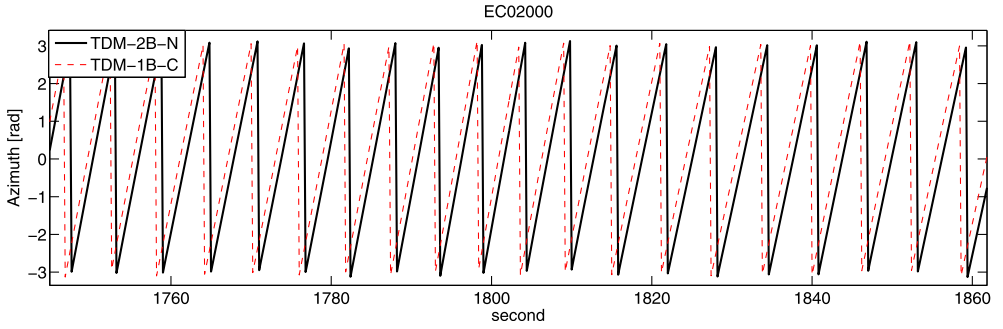

Fig. 19. An example of the time series of the azimuth angle of the TDM-1B-C and TDM-2B-N, EC02000.

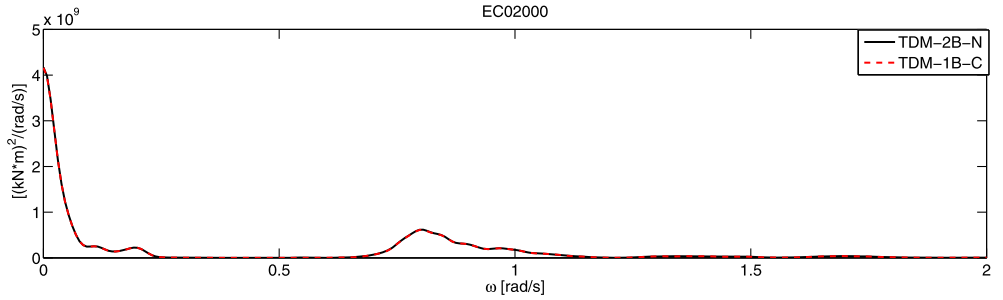

Fig. 20. Spectral densities of the fore-aft bending moment at the tower base of the TDM-1B-C and TDM-2B-N, EC02000.

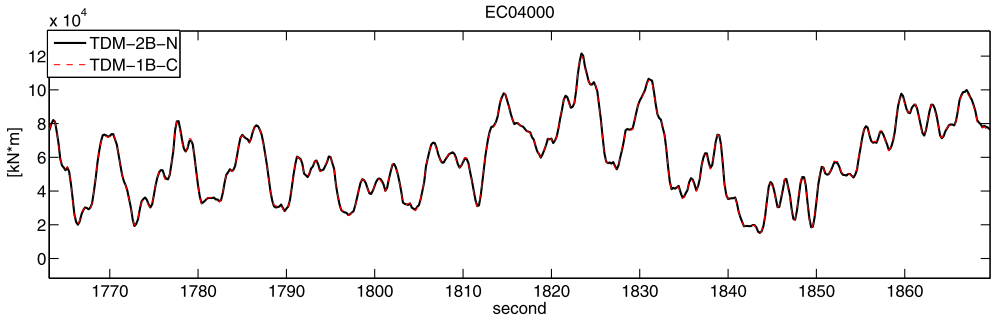

Fig. 21. An example of the time series of the fore-aft bending moment at the tower base of the TDM-1B-C and TDM-2B-N, EC04000.

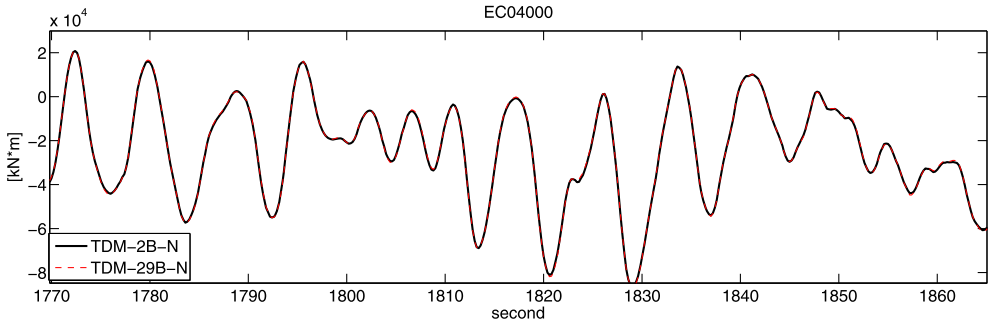

Fig. 22. An Example of the time series of the M_y (bending moment) of the TDM-2B-N and TDM-29B-N, EC04000.

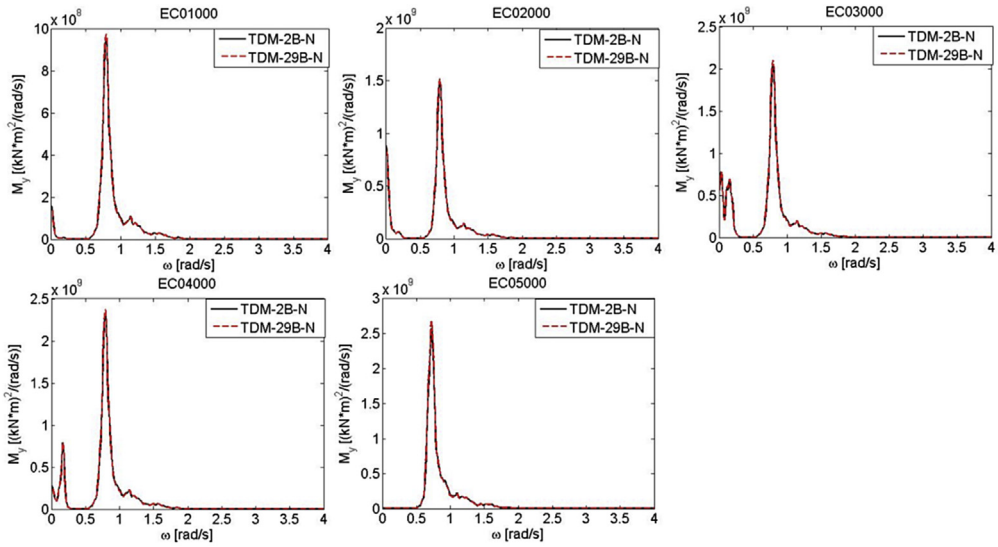

Fig. 23. Spectral densities of the M_y (bending moment) of the TDM-2B-N and TDM-29B-N in EC01000, EC02000, EC03000, EC04000 and EC05000.

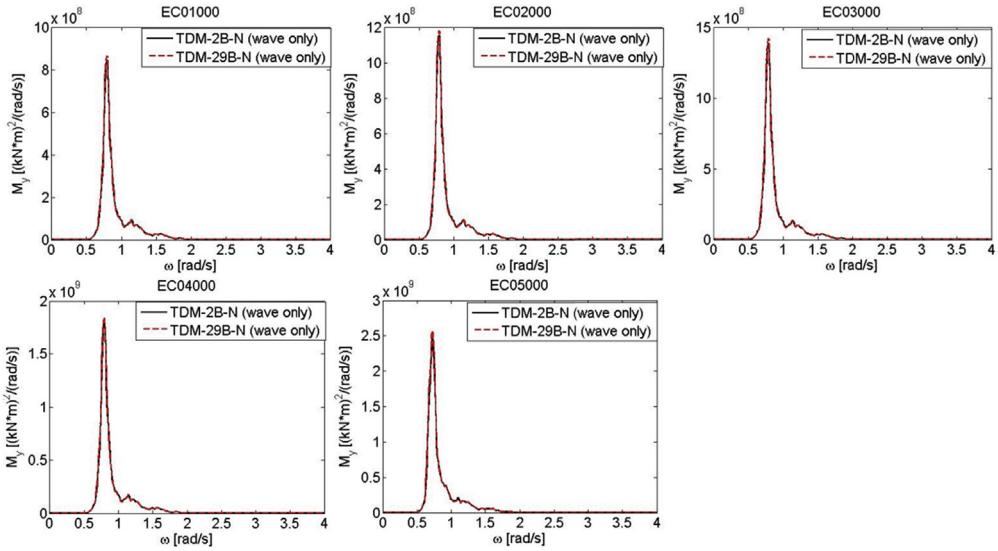

Fig. 24. Spectral densities of the M_y (bending moment) of the TDM-2B-N and TDM-29B-N in EC01000, EC02000, EC03000, EC04000 and EC05000 (wave only).

Acknowledgement

The authors acknowledge the financial support provided by the Research Council of Norway through the Centre for Ships and Ocean Structures (146025); the Norwegian Research Centre for Offshore Wind Technology (NOWITECH), NTNU (193823); and the Centre for Autonomous Marine Operations and Systems (AMOS) (223254), NTNU.

References

[1] Jonkman J. Definition of the floating system for phase iv of OC3. NREL/TP-500–47535. Golden, CO, USA: National Renewable Energy Laboratory; 2010.
[2] Nielsen FG, Hanson TD, Skaare B. Integrated dynamic analysis of floating offshore wind turbines. In: Proceedings of the 25th International conference on offshore mechanics and arctic engineering, OMAE2006–92291, Hamburg, Germany; 2006.
[3] Bachynski EE, Moan T. Design considerations for tension leg platform wind turbines. Mar Struct 2012;29:89–114.
[4] Matha D. Model development and loads analysis of an offshore wind turbine on a tension leg platform, with a comparison to other floating turbine concepts. Master's thesis. University of Colorado-Boulder; 2009 [April].
[5] Moon III WL, Nordstrom CJ. Tension leg platform turbine: a unique integration of mature technologies. In: Proceedings of the 16th offshore Symposium, Texas section of the society of Naval architects and marine engineers; 2010. A25–34.
[6] Henderson AR, Argyriadis K, Nichos J, Langston D. Offshore wind turbines on TLPs - assessment of floating support structures for offshore wind farms in German waters. In: 10th German wind energy conference, Bremen, Germany; 2010.
[7] Sclavounos P, Tracy C, Lee S. Floating offshore wind turbines: responses in a seastate; Pareto optimal designs and economic assessment. Tech. rep. Department of Mechanical Engineering, Massachusetts Institute of Technology; 2007.
[8] Botta G, Casale C, Lembo E, Serri L, Viani S. Resource and technology assessment for evaluating Italy's offshore wind energy potential. In: 2009 International conference on clean electrical power, capri, Italy; 2009. p. 507–13.
[9] Stewart G, Lackner M, Robertson A, Jonkman J, Goupee A. Calibration and validation of a FAST floating wind turbine model of the DeepCwind scaled tension-leg platform. In: Twenty-second International offshore and Polar engineering conference, Rhodes, Greece, vol. 1; 2012. p. 380–7. no. NREL/CP-5000-54822.
[10] Roddier D, Cermelli C, Aubault A, Weinstein A. WindFloat: A floating foundation for offshore wind turbines. J Renew Sustain Energy 2010;2:033104. http://dx.doi.org/10.1063/1.3435339.
[11] Roddier D, Peiffer A, Aubault A, Weinstein J. A generic 5 MW WindFloat for numerical tool validation & comparison against a generic spar. In: 30th International conference on ocean, offshore and arctic engineering, no, OMAE2011–50278, rotterdam, The Netherlands; 2011.
[12] Robertson A, Jonkman J, Masciola M, Song H, Goupee A, Coulling A, et al. Definition of the semisubmersible floating system for phase ii of OC4. In: Offshore code comparison collaboration continuation (OC4) for IEA Task 30; 2012.
[13] Huijs F, Mikx J, Savenije F, Ridder E. Integrated design of floater, mooring and control system for a semisubmersible floating wind turbine. Frankfurt: European Wind Energy Association (EWEA) Offshore; 2013.
[14] Drtechn Olav Olsen AS, (2016), http://www.olavolsen.no/en/node/17, accessed 2nd.May.2016.
[15] Luan C, Gao Z, Moan T. Design and analysis of a braceless steel 5-mw semi-submersible wind turbine. In: Proceedings of the 35th International conference on ocean, offshore and arctic engineering, OMAE2016–54848, Busan, Korea, June 19–24; 2016.
[16] Viselli AM, Goupee AJ, Dagher H. Model test of a 1:8 scale floating wind turbine offshore in the Gulf of Maine. In: 33th International conference on ocean, offshore and arctic engineering, no, OMAE2014-23639, san Francisco, CA, USA; 2014.
[17] The HiPRWind project, (2016), http://hiprwind.eu/, accessed 2nd.May.2016.
[19] DNV. Recommended Practice – buckling strength of plated structures. DNV-RP-C201, Det Norske Veritas. 2010.
[20] Norway Standards. Design of steel structures. NORSOK STANDARD N-004, Standards Norway. 2004.
[21] Nejad AR, Bachynski EE, Kvittem MI, Luan C, Gao Z, Moan T. Stochastic dynamic load effect and fatigue damage analysis of drivetrains in land-based and TLP, spar and semi-submersible floating wind turbines. Mar Struct 2015;42:137–53.
[22] Robertson A, Jonkman J, Qvist J, Chen X, Armendariz JA, Soares CG, et al. Offshore code comparison collaboration, continued: phase II results of a floating semisubmersible wind system. In: Proceedings of the 33rd International conference on ocean, offshore and arctic engineering, no. OMAE2014-24040, san Francisco, USA, 2014; 2014.
[23] Faltinsen OM. Sea loads on ships and offshore structures. UK: Cambridge University Press; 1990.
[25] Naess A, Moan T. Stochastic dynamics of marine structures. UK: Cambridge University Press; 2013.
[26] DNV. Sesam user manual HydroD. 2013.
[27] MARINTEK. SIMO User's manual. 2011.
[28] MARINTEK. RIFLEX User's manual. 2013.
[29] Ormberg H, Passano E, Luxcey N. Global analysis of a floating wind turbine using an aero-hydro-elastic model. Part 1: code development and case study. In: 30th International conference on ocean, offshore, and arctic Engineering,no, OMAE2011-50114, rotterdam, Netherlands; 2011.
[30] Luxcey N, Ormberg H, Passano E. Global analysis of a floating wind turbine using an aero-hydro-elastic numerical model. Part 2: benchmark study. In: 30th International conference on ocean, offshore, and arctic Engineering,no, OMAE2011-50088, rotterdam, Netherlands; 2011.
[31] Ormberg H, Bachynski EE. Global analysis of floating wind turbines: code development, model sensitivity and benchmark study. In: 22nd International ocean and Polar engineering conference, vol. 1; 2012. p. 366–73.
[32] Moriarty PJ, Hansen AC. AeroDyn theory manual. Tech. Rep, NREL/TP-500–36881. 2005.
[33] DNV. DNV-RP-C205, Det Norske Veritas. Recommended practice - environmental conditions and environmental loads. 2010.
[34] Li L, Gao Z, Moan T. Joint Distribution of Environmental Condition at Five European Offshore Sites for Design of Combined Wind and Wave Energy Devices. J Offshore Mech Arct Eng 2015;137(3):031901. http://dx.doi.org/10.1115/1.4029842 (16 pages).
[35] Cordle A, Jonkman J. State of the art in floating wind turbine design tools. In: Proceedings of the 21st International offshore and Polar engineering conference, Maui, Hawaii, USA, vol. 1; 2011. p. 367–74.
[36] Matha D, Schlipf M, Cordle A, Pereira R, Jonkman J. Challenges in Simulation of Aerodynamics, Hydrodynamics, and Mooring-Line Dynamics of Floating Offshore Wind Turbines. In: Proceedings of the 21st International offshore and Polar engineering conference, Maui, Hawaii, USA, vol. 1; 2011. p. 421–8.
[37] Kvittem MI, Moan T. Time domain analysis procedures for fatigue assessment of a semi-submersible wind turbine. Mar Struct 2015;40:38–59.
[38] IEC. Wind turbines – Part 1: design requirements. IEC-61400–1. International Electrotechnical Commission; 2005.
[39] IEC. Wind turbines: Part 3: design requirements for offshore wind turbines. IEC-61400–3. International Electrotechnical Commission; 2009.
[40] Karimirad M, Moan T. Wave and wind induced dynamic response of a spar-type offshore wind turbine. J Waterw Port Coast Ocean Eng 2012;138(1):9–20.
[41] Bae YH, Kim MH. Coupled dynamic analysis of multiple wind turbines on a large single floater. J Ocean Eng 2014;92:175–87.
[42] Bagbanci H, Karmakar D, Guedes Soares C. Comparison of Spar-Type and Semi-Submersible Type Floaters Concepts of Offshore Wind Turbines Using Long-Term Analysis. ASME J Offshore Mech Arct Eng 2015;137(6):061601.
[43] Moan T. Recent development of analysis and design of offshore wind turbines for deep water. In: Renewable energies offshore - 1st International conference on renewable energies offshore, RENEW 2014, Lisbon, Portugal; 2015.

[44] Debruyne Y, Alves M, Sarmento A. Efficient time-domain simulation of the performances of a floating offshore wind farm. In: Renewable energies offshore - 1st International conference on renewable energies offshore, RENEW 2014, Lisbon, Portugal; 2015.
[45] Mazarakos TP, Manolas DI, Grapsas T, Mavrakos SA, Riziotis VA, Voutsinas SG. Conceptual design and advanced hydro-aero-elastic modeling of a TLP concept for floating wind turbine applications. In: Renewable energies offshore - 1st International conference on renewable energies offshore, RENEW 2014, Lisbon, Portugal; 2015.
[46] Bachynski EE, Etemaddar M, Kvittem MI, Luan C, Moan T. Dynamic analysis of floating wind turbines during pitch actuator fault, grid loss, and shutdown. Energy Procedia 2013;35:210–22. http://dx.doi.org/10.1016/j.egypro.2013.07.174.
[47] Bachynski EE. Design and dynamic analysis of tension leg platform wind turbines. Ph.D thesis. Trondheim, Norway: Norwegian University of Science and Technology; 2014.